DYNAMIC SHEAR DEFORMATION IN ZINC CRYSTALS

Thesis by

Kenneth Robert King

In Partial Fulfillment of the Requirements
For the Degree of
Doctor of Philosophy

California Institute of Technology
Pasadena, California
1962

TABLE OF CONTENTS

ACKNOWLEDGEMENTS

The author wishes to express his thanks to Professor D. S. Wood and Professor D. S. Clark, who directed this research, for their guidance and support, as well as for their patience. Professor T. Vreeland, Jr., contributed many valuable suggestions during the course of this research and his continuing interest and assistance is appreciated. Mr. K. H. Adams and Mr. R. C. Brandt were especially helpful in providing advice and instruction in the proper techniques for obtaining etch-pip observations in zinc.

The author is indebted to the Union Carbide Corporation and the Shell Oil Company for fellowship grants. The course of the experimental work was greatly facilitated by a grant from the American Society for Testing and Materials which was employed to purchase one of the oscilloscopes. The testing program was conducted under a contract with the U. S. Army Research Office (Durham). Appreciation is extended to this agency for support of this work.

ABSTRACT

The initial stages of yielding in single crystals of zinc have been investigated at temperatures of -292°F (-180°C), -93°F (-70°C) and +75°F (24°C), by means of rapidly applied constant stress pulses to produce slip along the basal planes of these crystals.

The experimental results are interpreted in terms of a dislocation mechanism based upon the assumptions that the average velocity of dislocations remains constant during the period of constant applied stress and that the density of moving dislocations increases in linear proportion to the plastic strain. The experimental curves of plastic strain vs. time exhibit the form predicted by the assumed dislocation mechanism. The average dislocation velocity is found to be proportional to the 2.5 power of the excess of the applied stress over the static yield stress. The purity of the specimen and the test temperature are found to influence the average dislocation velocity only through their influence upon the static yield stress.

These results show that the behavior of basal slip dislocations in zinc is qualitatively the same as the behavior of slip dislocations in lithium fluoride and silicon-iron, as reported by Johnston and Gilman and by Stein and Low, respectively. Hence it is concluded that the concept of a lattice resistance to dislocation motion proposed by Gilman to explain the observed behavior of lithium fluoride and silicon-iron can be applied equally well to explain the observed behavior of zinc, and in fact that this is the only explanation consistent with the observed results.

LIST OF TABLES

LIST OF FIGURES

I. INTRODUCTION

The dislocation concept was first introduced into the field of crystal plasticity nearly thirty years ago. Since that time it has won universal acceptance and has been employed as the basis for the explanation of a wide variety of experimentally observed phenomena. However, it is only in the last ten to fifteen years that workers have begun to find techniques to isolate and study individual dislocations. Thus, although the experimental evidence strongly supported the case for the existence of dislocations, very little was known about their individual properties. Attempts to describe the macroscopic plastic deformation of crystals, and of polycrystalline materials as well, in terms of these poorly defined entities led to many conflicting theories based upon differing assumptions as to their individual and collective properties. As more is learned about the properties of the individual dislocations, it becomes possible to resolve some of these questions and to eliminate some of the theories.

Macroscopic plastic flow depends on how many dislocations are moving in a crystal and on how fast they are moving. In the past, it was assumed that the dislocations were not severely limited in velocity, except as the velocity of shear waves in the crystal was approached, and that the plastic flow was thus limited mainly by the available supply of dislocations. For this reason, efforts to explain the plastic yielding of crystals have been largely centered around mechanisms requiring the activation of some source of dislocations, such as a Frank-Read

source or dislocations pinned by Cottrell atmospheres or Peierls-Nabarro forces. Various efforts were made to explain the observed flow behavior in terms of intersections between the moving dislocations and other dislocations and defects in the crystal lattice but these explanations were often found to be inadequate.

Three years ago, however, Johnston and Gilman (1)* were able to measure, for the first time, the mobilities of individual dislocations. Dislocations in lithium fluoride crystals were caused to move by the application of stress pulses. Etch-pit techniques were used to locate the dislocations before and after their movements. It was found that dislocations in lithium fluoride accelerate very quickly and then move with constant velocity if a constant stress is applied to them. Below a certain stress, no dislocation motion occurs, but once having begun to move, dislocations increase their rates of motion very rapidly with further increases in the applied stress. At the lower stresses, corresponding to low dislocation velocities, the dislocation velocity increases approximately as the twenty-fifth power of the applied stress.

These observations led Gilman (2) to the conclusion that there is a quasi-viscosity or "plastic resistance" associated with dislocation motion in lithium fluoride. Gilman also showed that the macroscopic yield stress of a crystal could be explained on the basis of its plastic resistance. This was done by showing that a definite correlation exists

---

* Numbers appearing in parentheses refer to references listed at the end of this thesis.

between the yield stresses of different lithium fluoride crystals, or crystals subjected to different treatments, and the stress that is needed to make dislocations move in them at a certain velocity. Specifically, it has been found that the difference in stress required to produce the same dislocation velocity in two crystals is just equal to the difference in their yield stresses (1, 3). Finally, Gilman showed that the flow stress of crystals varies in a systematic way with the lattice structure of the crystal, with the elastic modulus, with the glide planes on which the dislocations move, and with the electronic structure or chemical bond type of the crystal. In this way, the plastic resistance of the crystal was related to the lattice structure and to the core structures of the dislocations.

Stein and Low (4) have used techniques similar to those used by Gilman and Johnston to observe the mobility of edge dislocations in silicon-iron crystals, and have found that these crystals exhibit plastic resistance and behave qualitatively much like lithium fluoride. Thus, in two rather different types of crystals, there is now direct evidence that plastic resistance controls plastic flow. Gilman (2) presents a strong argument that this is true for all crystals. If so, then the earlier mechanisms, such as Cottrell locking, Frank-Read sources, and the various dislocation intersection mechanisms, while still valid, will no longer be assumed to dominate the flow behavior. The adoption of this concept of plastic resistance will by no means solve all of the problems, since at present there is no theory to explain the cause of this plastic resistance.

To investigate the applicability of the plastic-resistance concept to other materials, the mobilities of individual dislocations in these materials should be studied. In addition, the macroscopic yield behavior of these materials should be re-examined in the light of the plastic-resistance concept to determine whether an interpretation on this basis presents an acceptable alternative to previously suggested interpretations. An application of the plastic-resistance concept to macroscopic yield behavior is illustrated by the following example.

A distinct delay time has been observed for the initiation of yielding under constant stress in polycrystalline steel (5) and molybdenum (6) (body centered cubic metals). An initial preyield microstrain, attributed to the build-up of dislocations at the grain boundaries (7), is followed by a rapid increase in both strain and strain rate as the dislocations are able to break through the grain boundaries and cause macroscopic yielding in the specimen. Recent studies (8) indicate that the presence of grain boundaries is necessary for the existence of the delayed yield phenomenon in steel. Evidence to the contrary has been presented by Kramer and his co-workers (9, 10, 11, 12), however. They have reported the existence of delayed yielding in single crystals of iron and β-brass (b.c.c.), zinc (h.c.p.), and in prestrained aluminum and copper (f.c.c.).

The behavior observed in single crystals may be the result of a different mechanism than the one causing the delayed yield in polycrystalline materials, however. An examination of a strain vs. time record for an aluminum single crystal (11) indicates that the plastic strain rate may increase continuously with time under constant stress

during the early stages of plastic deformation. In this case the definition of a delay time depends upon the arbitrary choice of the magnitude of plastic strain that defines the beginning of macroscopic yielding. This differs considerably from the case of polycrystalline steel. The delay time for yielding in steel is defined by the transition from a period in which the strain rate is slowly decreasing to one in which it increases rapidly and quickly reaches a large value. If the dislocation velocities in the crystals studied by Kramer are strongly dependent upon stress, as they are in lithium fluoride and in silicon-iron, then the apparent delay time reported by Kramer might be explained in terms of the time required for a sufficient amount of dislocation motion to produce a measurable plastic strain. Thus, a combination of the plastic resistance concept with some type of dislocation multiplication process might provide a more reasonable interpretation of this phenomenon.

The purpose of the present investigation is to learn more about the yield mechanism in zinc single crystals by means of rapid loading experiments, and to determine whether the concept of a plastic resistance, as observed in lithium fluoride and in silicon-iron, can be applied to the observed behavior of zinc. This is accomplished by experiments in which macroscopic strain is measured as a function of time while the crystal is subjected to a constant stress. Etch-pip*

* An etch-pip is an etch figure which is formed at the point where a dislocation intersects the surface of a crystal. In many cases these figures correspond to small depressions or pits in the surface and are therefore referred to as "etch-pits". The technique employed in the present experiments produces hillocks instead of depressions. Thus the name "etch-pips" is employed.

observations are employed to determine the number of dislocations taking part in the plastic flow. The stress dependence of the average dislocation velocity can then be deduced from these measurements. The effects of temperature and impurities in the zinc crystals upon the results are investigated. The possible existence of a delay time for yielding is also considered.

Considerable care has been taken to develop a method of loading which gives a sufficiently uniform stress distribution to obtain a well-defined yield point under static testing conditions. This point is emphasized because previous work (13, 14) has shown that the sharply defined static yield stress in zinc single crystals is easily suppressed by small stress concentrations. Such stress concentrations also are likely to affect the yield behavior under dynamic loading conditions.

II. MATERIAL AND SPECIMEN PREPARATION

Zinc crystals of three purities were investigated: 1) 99.999 per cent; 2) 99.99 per cent; and 3) 99.99 per cent with nitrogen added. The addition of nitrogen was accomplished by bubbling gaseous nitrogen through the melt for 10 hr.

Spherically shaped single crystals 1-3/4 in. in diameter were grown in vacuo in graphite coated pyrex glass molds by means of the procedure described by Stofel (15). Cylindrical specimens 1 in. in diameter and 1 in. long were cut from these spherical crystals by means of acid machining techniques in order to avoid damage to the crystals. The orientation of the specimen with respect to the crystallographic axes was chosen so that both the slip plane (0001) and slip direction $<2\bar{1}\bar{1}0>$ of the crystal were inclined at 45° to the cylinder axis, as shown in Fig. 1. Thus when a given axial compressive stress was applied to the cylinder the maximum possible resolved shear stress was obtained on a single slip system.

The details of the technique employed to produce test specimens of the desired orientation from the spherical crystals were as follows: First, the approximate orientation of the spherical single crystal was determined by etching with a 1:1 solution of hydrochloric acid and water. This etch produces six broad bands on the surface which meet at two common poles. The direction defined approximately by the diameter passing through these two poles is the hexagonal axis of the crystal structure. The crystal was then cooled, at a rate not exceeding

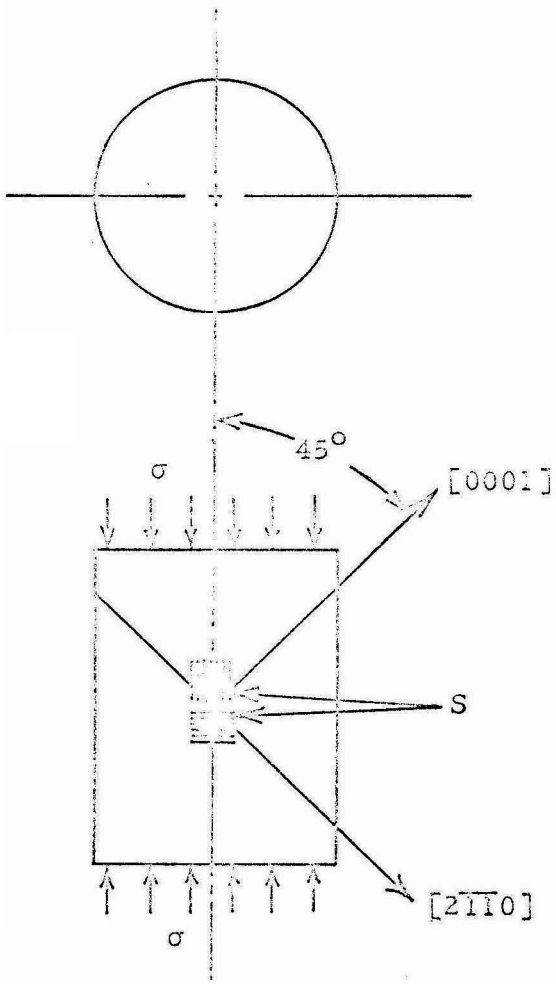

σ = Applied Stress

S = Strain Gages

[0001] = Hexagonal Crystal Axis

[2$\bar{1}\bar{1}$0] = Slip Direction

Fig. 1 Test Specimen.

5°F/min (3°C/min), to liquid nitrogen temperature. (This low cooling rate was employed in order to prevent plastic flow and the formation of cracks due to thermal stress.) Several thin chips were then successively removed from the surface at one of the poles by cleaving on the basal planes. A flat surface about 1 in. in diameter was thus obtained which served as a crystallographic reference surface. The slip direction was determined from observations of twin traces on the basal plane of removed chips.

After cleaving, the spherical crystal was cemented to a fixture which permitted a second flat surface to be machined at 45° to both the basal plane and the slip direction. An acid lapping wheel* was used for this operation. This new surface then became the reference surface for the machining of the cylindrical surface on an acid lathe.** This procedure produced a cylinder 1.000 in. in diameter and about 1-1/2 in. long. An acid saw*** was then employed to cut the specimen to within about 0.020 in. of the finished length. Finally, the sawed ends of the specimen were flattened with wet 600 silicon carbide paper, after which an additional 0.003 to 0.004 in. was removed with nitric

---

* The acid lapping wheel is a rotating disc which dips into a 1:1 nitric acid and water solution and rubs against the spherical crystal. The crystal is rotated about an axis perpendicular to the surface of the wheel as it is being lapped.

** The acid lathe has been described by Stofel (14).

*** The acid saw consists of a 0.005 in. diameter stainless steel wire which carries nitric acid into the cut as it is drawn back and forth. Acid is fed onto the wire by means of glass capillary plates attached to the fixture. The capillary plates also serve as guides for the wire.

acid. Examination under a microscope indicated that this last step was sufficient to remove the deformation introduced by the abrasive.

Since only the initial stages of yielding are being studied in this investigation, very little deformation is introduced into a specimen in a given test. For this reason, it is possible to perform repeated tests on the same specimen and thus to avoid errors arising from differences between specimens. After each test, the specimen is annealed at a temperature of 700°F (370°C) for one hr. Fresh strain gages are then attached and allowed to dry for at least two days at room temperature. To verify the effectiveness of this annealing treatment in returning the specimen to its original state, several static tests were performed on one specimen, annealing after each test. A systematic change in the yield stress was not observed in these tests, although random variations of 1 to 2 lb/in.^{2} were found to occur from one test to the next (see Figs. 5 and 6). Similar observations on the effect of annealing procedure were made by Li, Washburn and Parker (16).

A total of six specimens were studied: one nitrogen doped, one of 99.99 per cent purity, and four of 99.999 per cent purity.

III. EQUIPMENT AND TEST PROCEDURE

Stress Application

A shock tube is employed to apply a uniformly distributed pressure rapidly to one end of the cylindrical specimen. This shock tube is 31 ft. long, has an I.D. of 1-1/2 in., and is mounted in a vertical position as shown schematically in Fig. 2. The specimen faces the bottom end of the shock tube and is supported as shown in Fig. 3. The specimen rests on a flat stainless steel base, separated from it by a 0.002 in. layer of teflon to improve lubrication and load distribution. A thick-walled brass cylinder surrounds the specimen and is also supported by the stainless steel base. This cylinder supports a plate with a hole in it about 0.010 in. larger than the specimen diameter. The height of the brass cylinder can be adjusted so that the top surface of this plate is flush with the top surface of the specimen. A 0.002 in. thick teflon diaphragm covers both the plate and the specimen and is fastened to the end of the shock tube. Thus, the end of the shock tube is sealed while at the same time the shock pressure acts uniformly on the specimen. The stainless steel base rests in a copper box which serves as the container for liquid thermostatic baths. Beneath the copper box are three 1/2 in. thick glass plates for thermal insulation. The stainless steel base, copper box, and glass plates are all bolted to a heavy steel back-up block. This block is arranged to travel up and down on a short vertical track to permit installation of the specimen and positioning of it against the end of the shock tube.

To operate the shock tube, carbon dioxide gas from a high

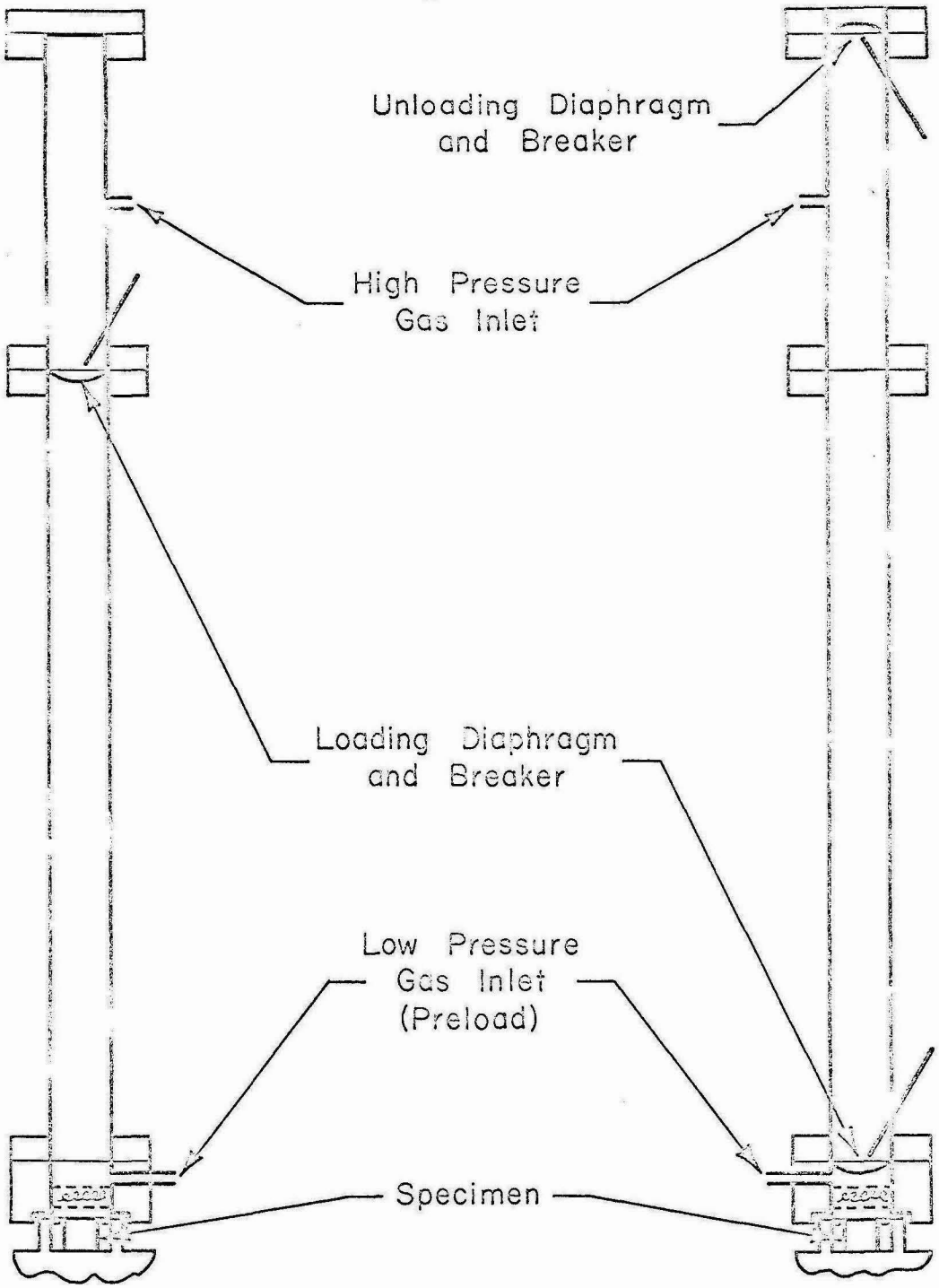

(a) Shock Tube Operation

(b) Quick-Opening Valve Operation

Fig. 2 Schematic View of Shock Tube Showing Methods for Applying Load Rapidly to Specimen.

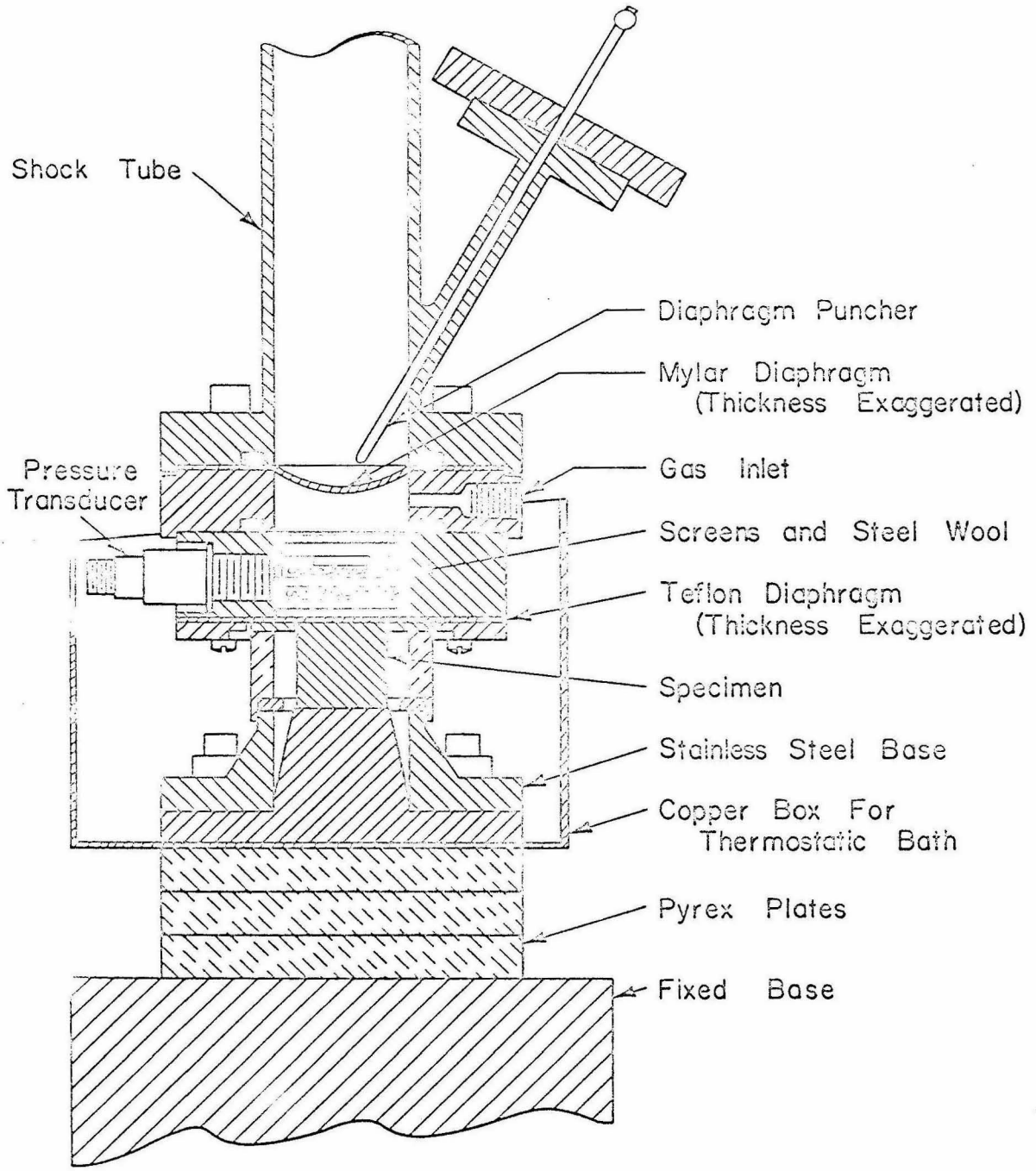

Fig. 3 Sectional View Showing Specimen in Position Facing End of Shock Tube.

pressure cylinder is admitted to the section of the tube above the thin mylar diaphragm near the top (see Fig. 2a) and the pressure is adjusted to some predetermined value. A 10 to 20 lb/in.^{2} preload pressure is also applied to the specimen by admitting nitrogen to the lower section of the tube. The diaphragm is then broken by means of a solenoid-operated puncher and a shock wave travels down the tube and reflects off the specimen, thus applying a uniformly distributed load. The load remains on the specimen until an unloading wave reaches it from the top end of the tube. Screens and steel wool are placed in the bottom end of the tube, just above the specimen, to prevent the pressure from rising so rapidly that elastic waves are excited in the specimen or its back-up support. The pressure rises to its final value in about 0.4 millisec and remains constant for about 10 millisec. Pressures up to about 125 lb/in.^{2} have been employed in these experiments. The equipment is capable of much higher pressures. Difficulties are encountered in maintaining a constant shock pressure on the specimen at the higher operating pressures, however.

When longer load durations are desired, the shock tube is operated as shown in Fig. 2b. The diaphragm is moved to a position just above the specimen, where it can be broken by another solenoid-operated puncher. In this case, there is no time for a shock front to build up and the pressure behind the diaphragm is the pressure that is applied to the specimen. Thus, the breaking diaphragm simply serves as a quick-opening valve. The pressure on the specimen rises to its

final value in about 0.8 millisec in this case and remains until released. Since repeated tests are made on the same crystal, it is usually desirable to release the pressure rather quickly in order to avoid deforming the specimen excessively. For this reason, the upper section of the tube is inverted so that the upper diaphragm-breaker faces the top of the tube. A delay circuit makes it possible to break the diaphragm at this end of the tube, thus releasing the load, at any desired time interval after the lower diaphragm has been broken. The total resolved shear strain produced in each test was limited to 0.1 per cent or less.

Measurements of Stress and Strain

The pressure acting on the specimen during a test is measured by means of a SLM Pressure Indicator manufactured by the Kistler Instrument Company. This device consists of a quartz piezo-electric pressure transducer and an amplifier unit. The transducer is located near the bottom end of the shock tube, just above the specimen. The output from this unit is displayed on one channel of a Tektronix 555 dual beam oscilloscope.

Four SR-4 type A-18 resistance strain gages are cemented to the specimen and connected together to form a bridge circuit. The strain measurements are obtained by amplifying the strain gage output by means of a high gain preamplifier on the other channel of the 555 oscilloscope. Usually, the strain gage output is also displayed at a different gain on a second oscilloscope. The oscilloscope sweeps are triggered by a contact closed during the motion of the diaphragm-

breaker. Polaroid cameras are used to record these signals. The total strain occurring during a test is also measured independently by means of a Baldwin Type-N Strain Indicator. A general view of the rapid load testing system is shown in Fig. 4.

Static Tests

Static tests are performed by bleeding gas slowly into the shock tube and recording the pressure as indicated on bourdon tube pressure gages together with the strain as indicated on the Baldwin Strain Indicator. This method does not produce the immediate drop in stress generally associated with a sharp yield point because the loading system is an extremely "soft" one. The pressure is reduced manually as soon as rapid yielding is observed, however. This usually prevents excessive strain in the specimen. If the strain is not excessive, the pressure is again increased slowly and additional strain readings are taken. Since these latter measurements generally show strain to be taking place at stresses below the upper yield stress, a drop in stress is actually observed in such cases, although not in the form obtained in the more conventional "stiff" testing machines. In the cases where the pressure is not increased again, the amount of strain which has taken place is itself an indication of the sharpness of the yield point and the associated drop in load.

Temperature Control and Measurement

The method employed to obtain the lower test temperatures ($-93^{\circ}F$ and $-292^{\circ}F$) varies somewhat with the nature of the cooling

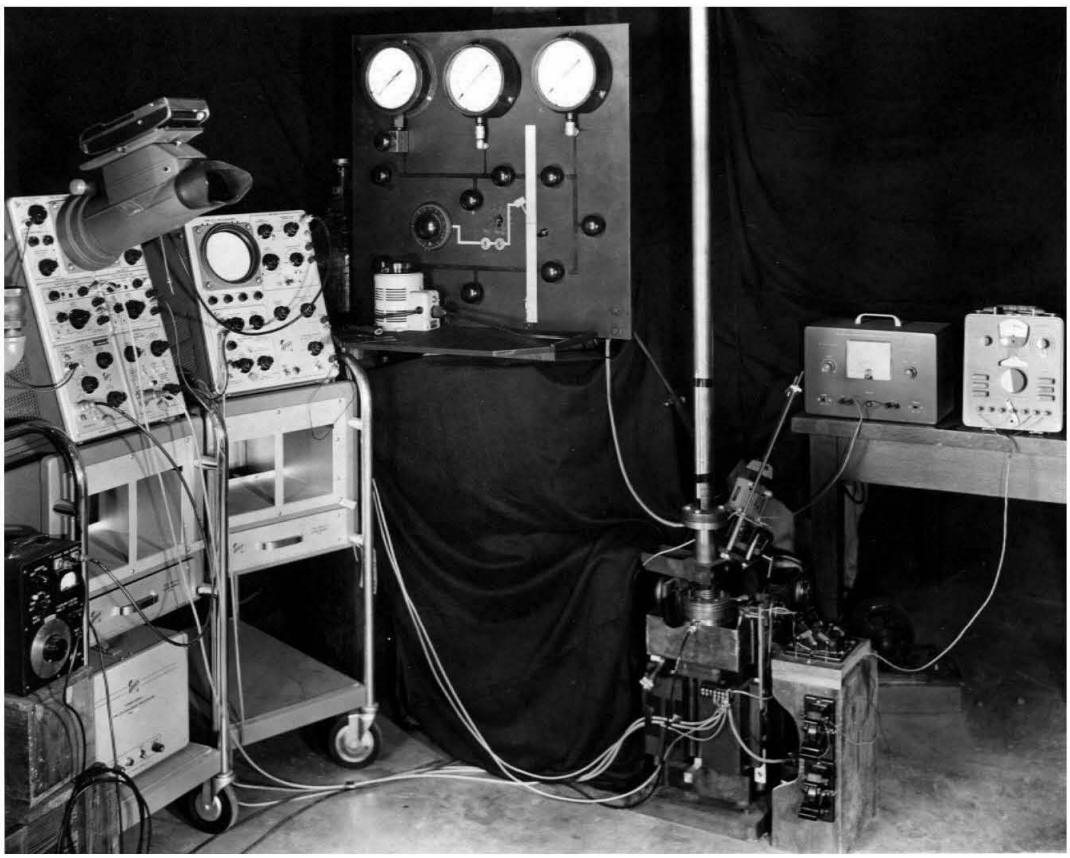

Fig. 4 General View of Rapid Loading System.

medium in each case, but the main features are the same. The specimen is first installed and raised into position facing the end of the shock tube, as in the room temperature (75°F) tests. The cooling medium is then introduced at a controlled rate into the copper box surrounding the specimen assembly. Cooling is achieved entirely by means of conduction through the stainless steel specimen support and by contact between the specimen and the cold gases in the box; the specimen is never submerged in the liquid coolant. The rate of cooling is limited to 5°F/min (3°C/min) or less in order to avoid plastic flow due to thermal stresses.

For the tests at -93°F, freon 11 ($CC\ell_3F$) is poured into the copper box to a depth of about 3/4 in. Freon 11 remains in the liquid state from 75°F to below -93°F and serves as a heat conducting medium between the specimen assembly and the dry ice which is used as the cooling medium. The specimen temperature is continuously monitored during the cooling process and dry ice is added at regular and frequent intervals in such amounts as are necessary to maintain the desired cooling rate. When the equilibrium temperature is reached, the bottom of the box is covered with dry ice.

For the tests at -292°F, liquid nitrogen is continuously dribbled into the copper box from one or more of three styrafoam containers. The cooling effect in this case is achieved by the vaporization of the nitrogen and through the nitrogen vapor itself. The rate of cooling is controlled by varying the rate at which liquid nitrogen is allowed to dribble into the box. When the equilibrium temperature is reached,

the bottom of the box is filled with liquid nitrogen to a depth of 1/2 to 3/4 in. The strain gages on the specimen are covered with small pieces of felt in order to eliminate high frequency thermal noise caused by contact with the nitrogen vapor.

Iron-constantan thermocouples are used to measure the temperatures in the neighborhood of the specimen. The accuracy of measurement is estimated to be $\pm 2^{\circ}F$. A brass dummy specimen, with thermocouples located in the center and on the top surface, was employed to determine the amount of temperature variation within the specimen and between the specimen and surrounding parts. The thermal conductivities of brass and zinc are approximately the same. A difference between the temperatures at these two positions in the specimen could not be detected at any stage during cooling or testing. The application of the preload pressure did not produce a measurable change in the temperature of the specimen. The maximum error in the measurement of temperature differences and temperature variations is $0.5^{\circ}F$.

A thermocouple located in the brass cylinder which surrounds the specimen was used to indicate the temperature of the specimen during the actual tests. The temperatures at this point were found to be about $5^{\circ}F$ cooler than the specimen itself during cooling and either 3 or $6^{\circ}F$ warmer than the specimen at the equilibrium temperature, depending upon the temperature of the test. The bottom end of the shock tube is considerably warmer than the specimen assembly because of the fact that there is no direct thermal contact between them. The

carbon dioxide or nitrogen gas in the copper box is somewhat warmer than it would otherwise be, however, so that the specimen temperature at equilibrium is 10 or 25°F warmer than the dry ice or liquid nitrogen. Once equilibrium is reached, the specimen temperature remains constant to within ± 1°F.

Method of Observing Dislocations

Observations of dislocation densities and distributions in annealed and deformed specimens provide a link between the macroscopic strain measurements and the behavior of individual dislocations. These observations are obtained by means of an etching technique developed by Brandt, Adams and Vreeland (17). The surface of the specimen is first prepared by chemical polishing, after which the specimen is dipped in a solution which introduces mercury to the surface. A subsequent polish results in the formation of small pips at each point where a dislocation intersects the surface. This technique reveals dislocations on $\{10\bar{1}0\}$ prism planes of zinc. The cylindrical surface of the specimen is tangent to $\{10\bar{1}0\}$ planes along two elements of the cylinder on opposite sides of the specimen from one another. These are the same positions at which the strain gages are attached to the specimen, as shown in Fig. 1. Good etch figures can be obtained on surfaces oriented within 5° of the $\{10\bar{1}0\}$ planes, so that dislocations in a band about 0.1 in. wide on each side of the specimen can be observed by this method.

Because of the effects of chemical polishing, a specimen cannot be tested again after etch-pip observations have been made on it, so

that these observations can only be made after the final test on a given specimen. Therefore, in order to obtain observations of the same specimen in both the deformed and annealed states, the deformed specimen is polished and etched immediately after its final test and photomicrographs are made of the areas of interest. Then the specimen is given a standard annealing treatment of one hr. at 700°F. It is annealed in vacuo, however, rather than in a hydrogen atmosphere, in order to remove as much of the mercury as possible from the surface. Finally, the specimen is repolished and re-etched to reveal the density and distribution of dislocations in the annealed state.

IV. EXPERIMENTAL RESULTS

Static Tests

Curves of resolved shear stress vs. resolved shear strain as determined by static tests are shown in Figs. 5, 6, and 7 for the nitrogen doped specimen, the specimen of 99.99 per cent purity, and one specimen of 99.999 per cent purity, respectively. Dashed lines are regions where the strain took place so rapidly that it was impossible to obtain readings on the strain indicator. Four tests were performed at 75°F (24°C) on the nitrogen doped specimen, and three at this same temperature on the specimen of 99.99 per cent purity. The curves for these tests are numbered in the order in which the tests were performed. These are the only two cases in which more than one static test was performed on a specimen at a given temperature. The curves shown in Fig. 7 for a specimen of 99.999 per cent purity are typical of the curves obtained for the four specimens of this purity which were tested.

The values obtained for the critical resolved shear stress in these tests are listed in Table I. The critical resolved shear stress is taken as the stress at the beginning of rapid straining for the cases in which a sharp yield point is exhibited. In all other cases, the plastic flow curve has been extrapolated back to zero plastic strain and the value of the stress at this point taken as the critical resolved shear stress.

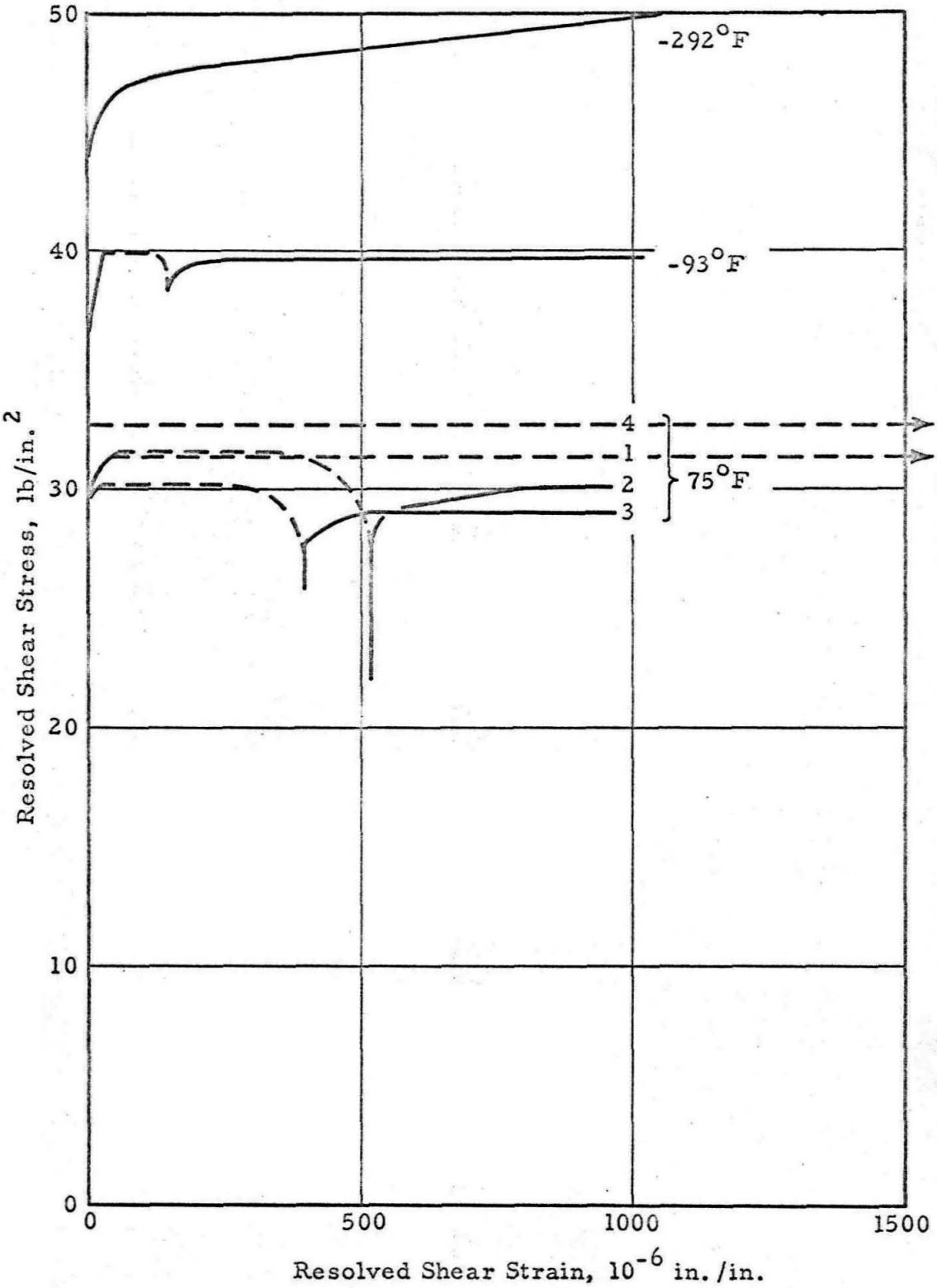

Fig. 5 Static Stress vs. Strain Curves for Nitrogen Doped Specimen.

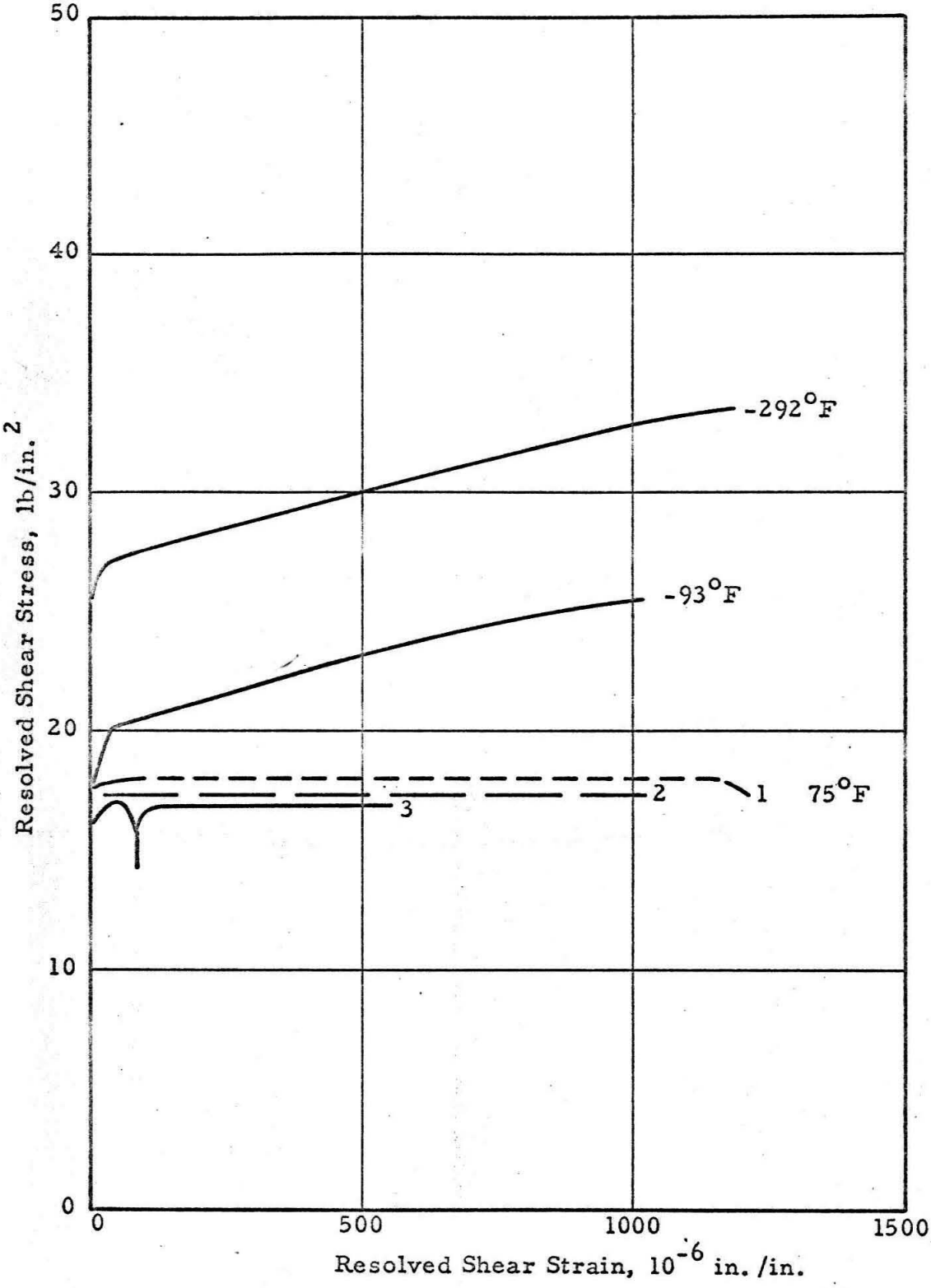

Fig. 6 Static Stress vs. Strain Curves for Specimen of 99.99 Per Cent Purity.

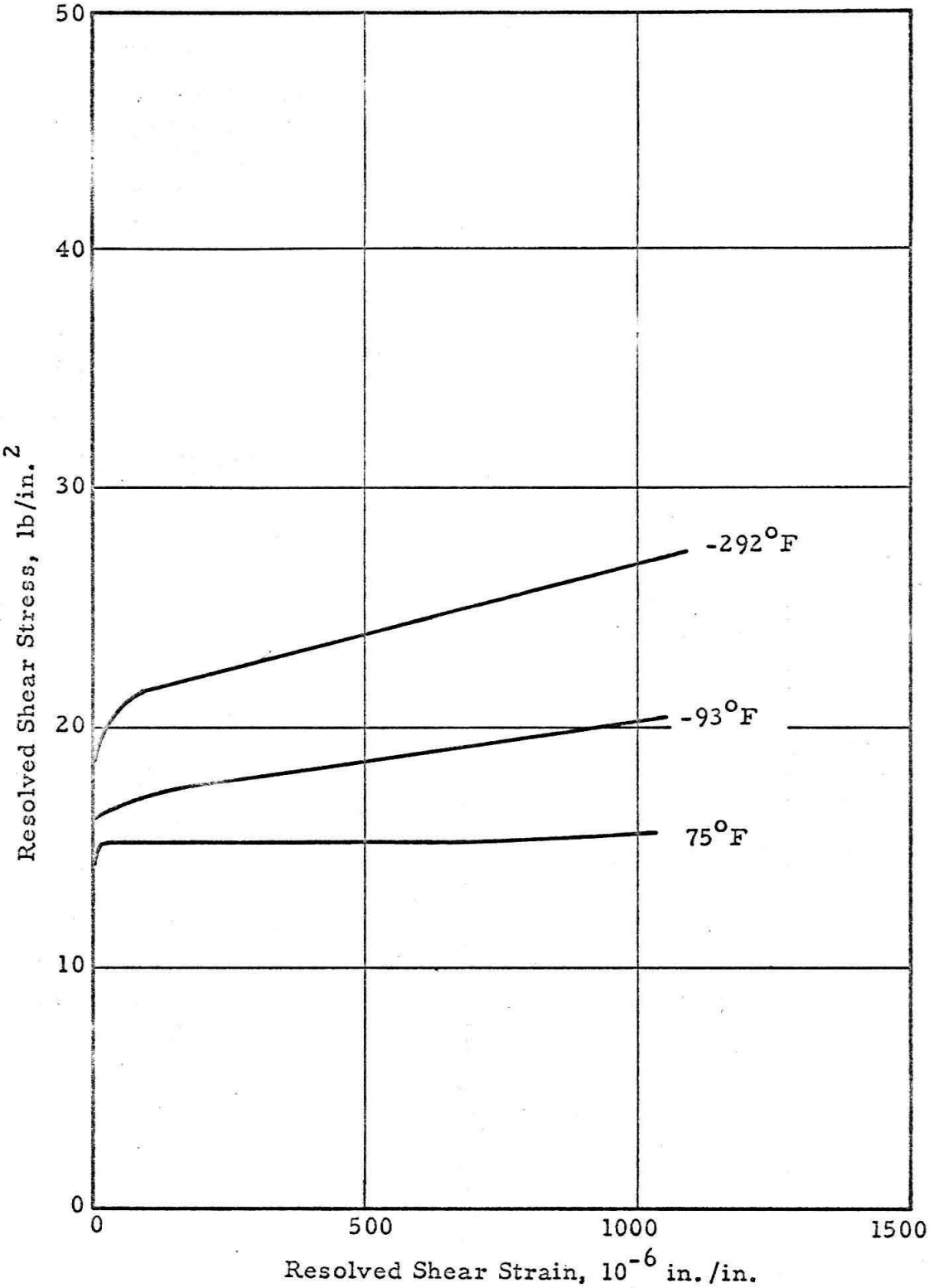

Fig. 7 Static Stress vs. Strain Curves for Specimen of 99.999 Per Cent Purity.

TABLE I

Critical Resolved Shear Stress in Static Tests

Specimen No.	Specimen Purity (per cent)	Temperature -292°F	-93°F	75°F
28	99.99 + nitrogen	47.3 lb/in.^{2}	40.0 lb/in.^{2}	31.5 lb/in.^{2} 31.6 lb/in.^{2} 30.2 lb/in.^{2} 32.7 lb/in.^{2}
30	99.99	27.1 lb/in.^{2}	20.1 lb/in.^{2}	18.0 lb/in.^{2} 17.3 lb/in.^{2} 17.0 lb/in.^{2}
36	99.999	--	--	16.2 lb/in.^{2}
37	99.999	--	--	15.1 lb/in.^{2}
38	99.999	21.1 lb/in.^{2}	16.5 lb/in.^{2}	15.2 lb/in.^{2}
39	99.999	21.1 lb/in.^{2}	16.5 lb/in.^{2}	15.2 lb/in.^{2}

Rapid Loading Tests

Typical records of rapid loading tests are shown in Fig. 8 for both the shock tube mode of operation and the quick opening valve mode. The initial level of the pressure vs. time signal corresponds to the preload on the specimen. The small step in the strain signal upon application of the load corresponds to the elastic strain in the crystal. The two small disturbances in the pressure vs. time curve of Fig. 8b are caused by an unloading pressure pulse, originating in the short "preload" section between the loading diaphragm and the specimen (see Fig. 2b). This pulse is propagated up and down the tube, after the diaphragm is broken, with a round trip time of about 70 millisec.

Graphs of plastic shear strain vs. time and strain rate vs. time, with both strain and strain rate plotted on a log scale, are shown in Fig. 9 for a rapid load test at 75°F on the nitrogen doped specimen. Similar graphs are shown in Fig. 10 for a rapid load test at -292°F on the same specimen. The results shown in these figures are typical of those obtained for the nitrogen doped specimen and for the specimen of 99.99 per cent purity. Graphs of plastic shear strain vs. time and strain rate vs. time for a test at 75°F on a specimen of 99.999 per cent purity are shown in Fig. 11. These are typical of the results obtained for tests on specimens of that purity.

Some tests were made to investigate the behavior under interrupted loading. An initial load was applied and removed in the usual manner. The same load was then repeated a short time later.

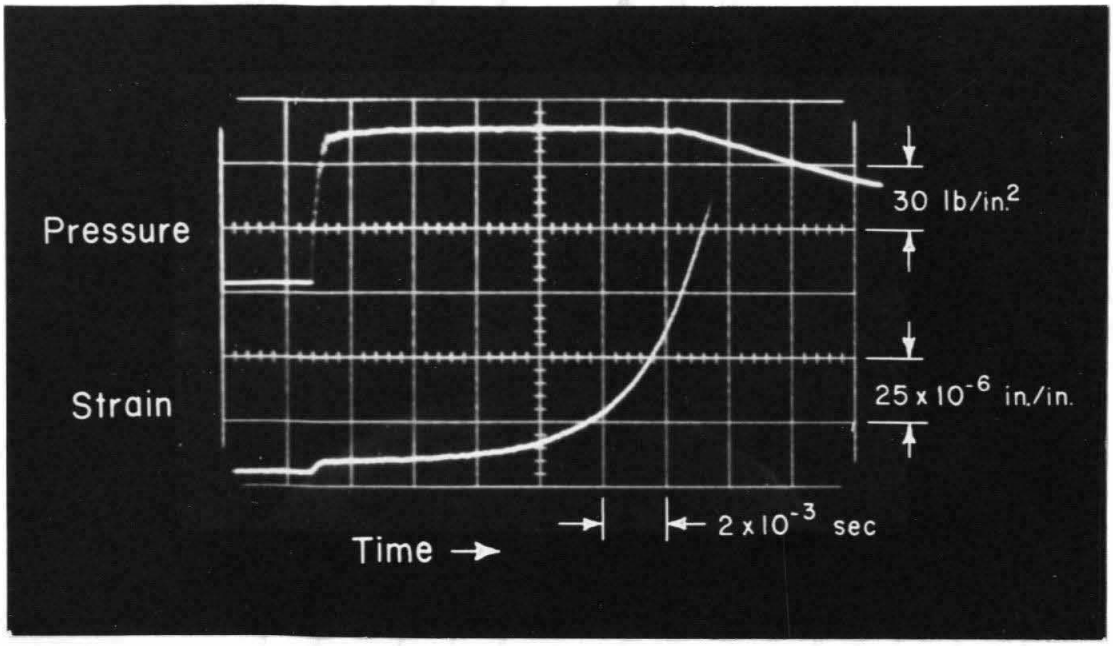

(a) Shock Tube Operation, 75°F.

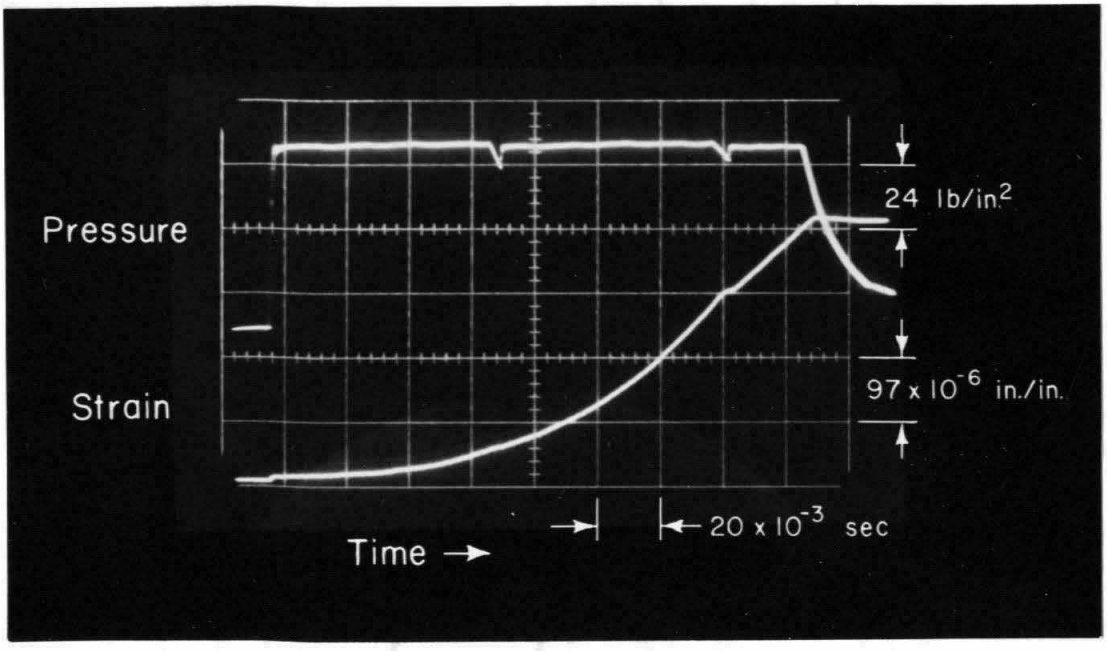

(b) Quick-Opening Valve Operation, -93°F.

Fig. 8 Oscilloscope Records of Rapid Loading Tests.

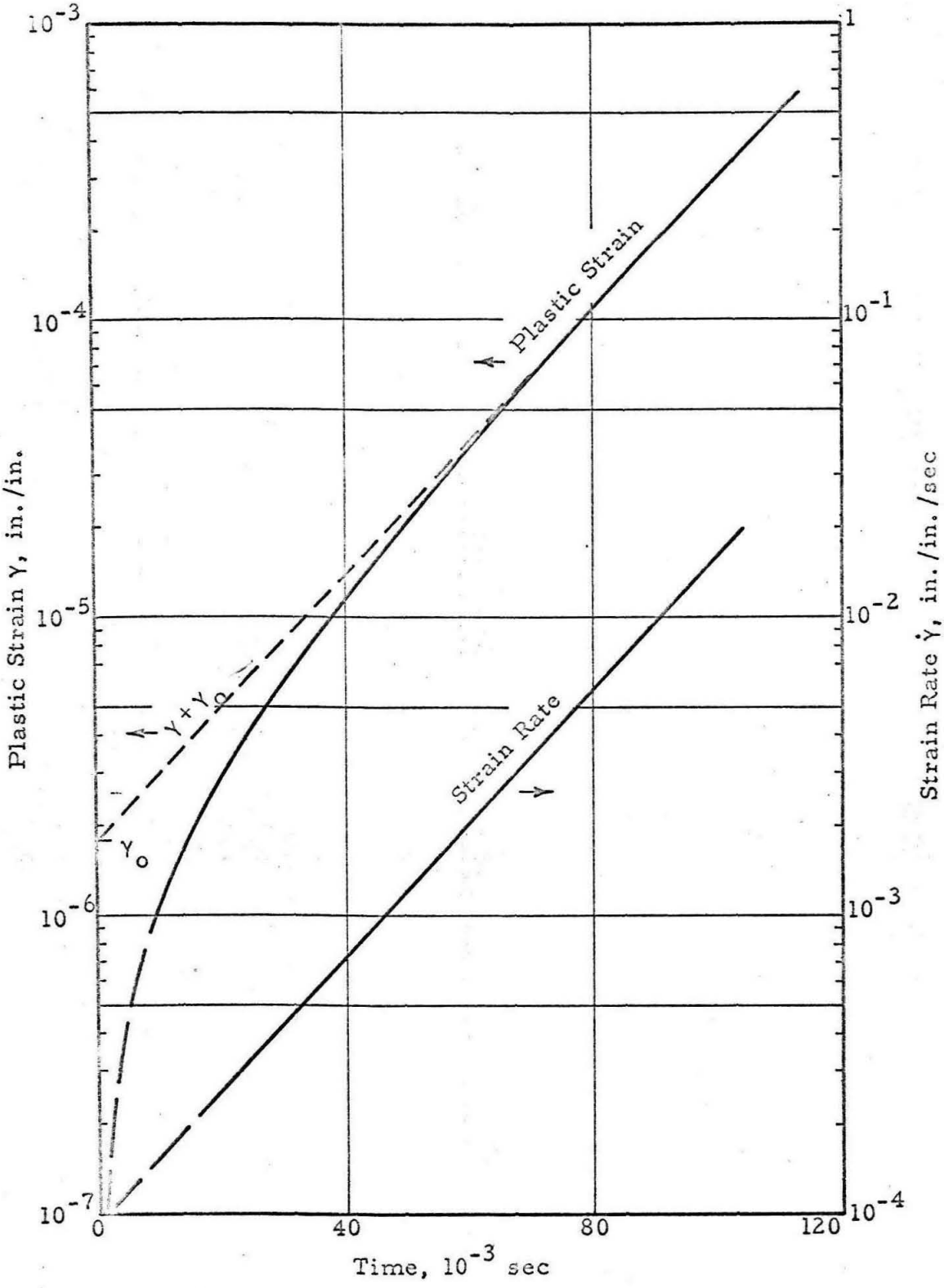

Fig. 9 Plastic Strain vs. Time and Strain Rate vs. Time. Nitrogen Doped Specimen, 75°F. Applied Resolved Shear Stress 37.4 lb/in.^{2}.

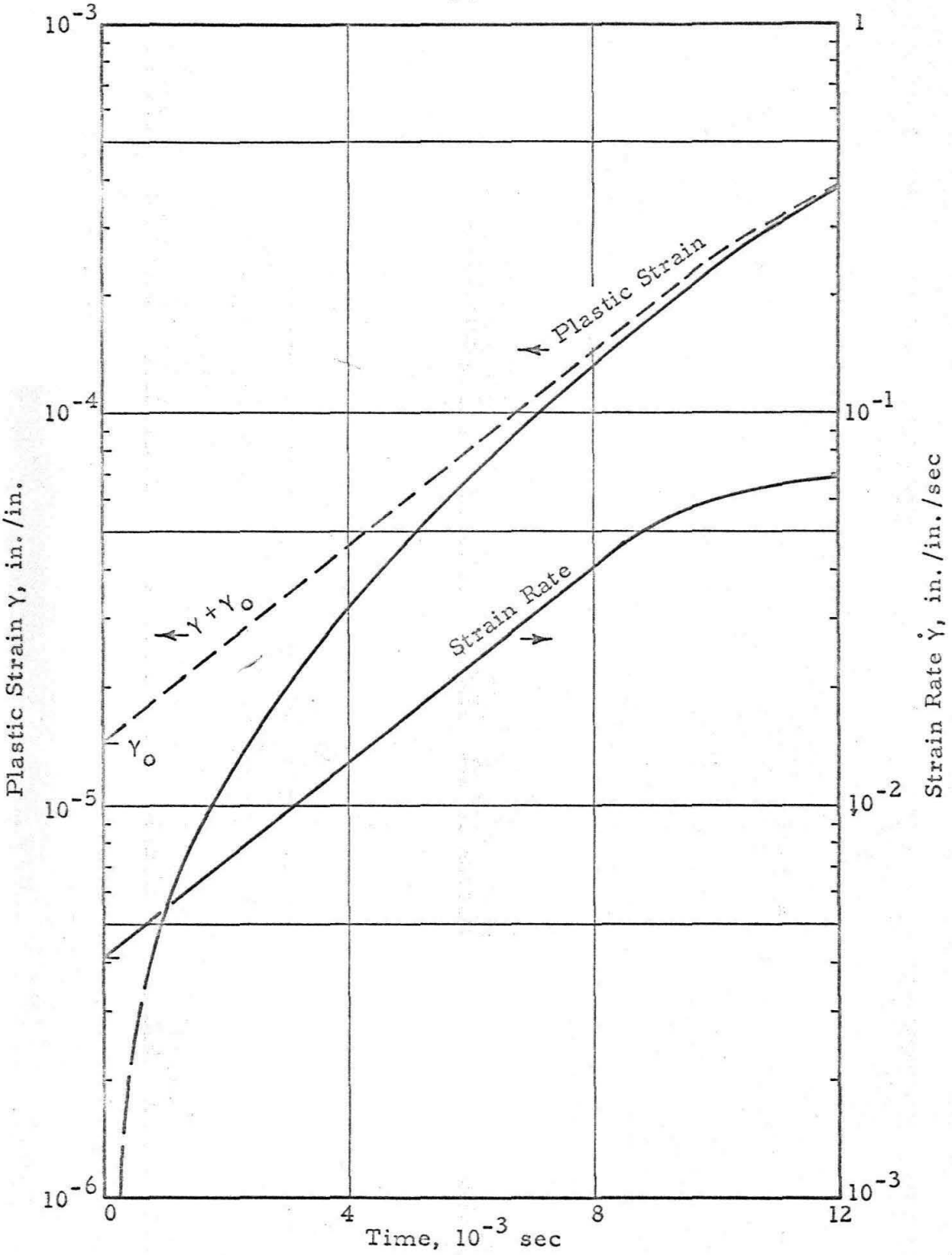

Fig. 10 Plastic Strain vs. Time and Strain Rate vs. Time. Nitrogen Doped Specimen, -292°F. Applied Resolved Shear Stress 63.3 lb/in.^{2}.

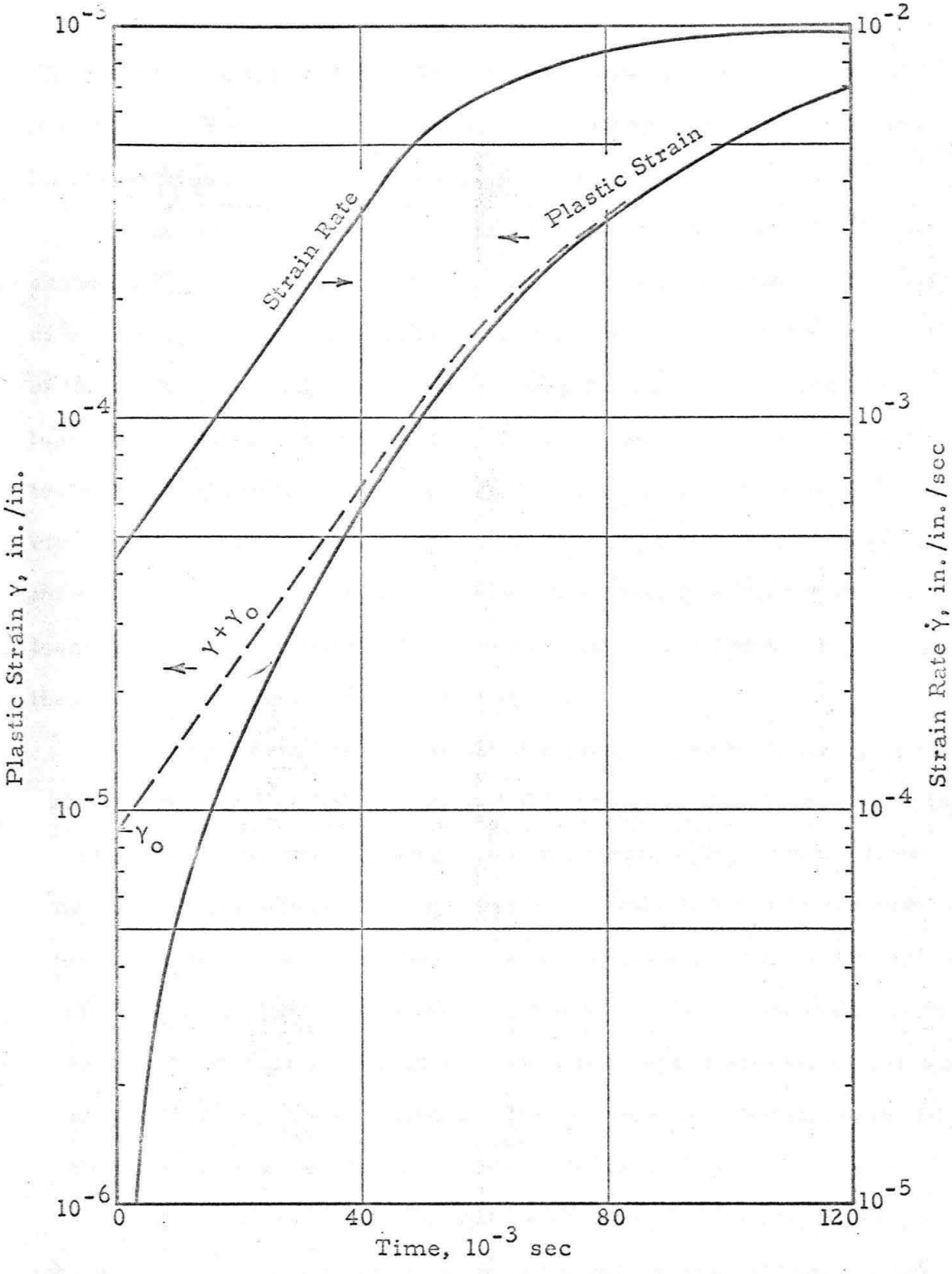

Fig. 11 Plastic Strain vs. Time and Strain Rate vs. Time. Specimen of 99.999 Per Cent Purity (No. 38), 75°F. Applied Resolved Shear Stress 20.2 lb/in.^{2}.

The results of a test in which this process was repeated five times are shown in Fig. 12. The short gaps in the two curves correspond to interruptions in loading of about 15 minutes each.

The results of a test of relatively long duration at -292°F are shown in Fig. 13. The periodic reductions in both magnitude and rate of increase of the strain rate coincide with the arrival at the specimen of the small unloading pulse which propagates up and down the shock tube. This effect was observed in all of the longer duration rapid load tests at -93°F and -292°F. However, it was not observed at +75°F in either this type of test or in tests of the type shown in Fig. 12. Only three tests of the latter type, each involving only one interruption in loading, were performed at the lower temperatures and the effect of the interruptions in these tests is not clear.

The complete results for all of the rapid load tests are given in Table II. These results are presented in terms of the slope, $k\bar{v}$, of the log strain rate vs. time curve and its intercept, $\rho_o b\bar{v}$, with the time = 0 axis. In cases where the slope was apparently affected by the low pressure pulses described above, the initial slope, prior to the arrival of the first disturbance, was taken as the best value. The static yield stress, τ_y, for each specimen and the applied shear stress, τ, are also tabulated. The τ_y values listed are the averages of the corresponding critical resolved shear stress values from Table I.

Figure 14 is a plot of the quantity log $k\bar{v}$ vs. log $(\tau-\tau_y)$, the increment of the applied resolved shear stress above the static yield stress for that test. The points for all of the tests fall along one line. The experimental scatter between these points is smallest for

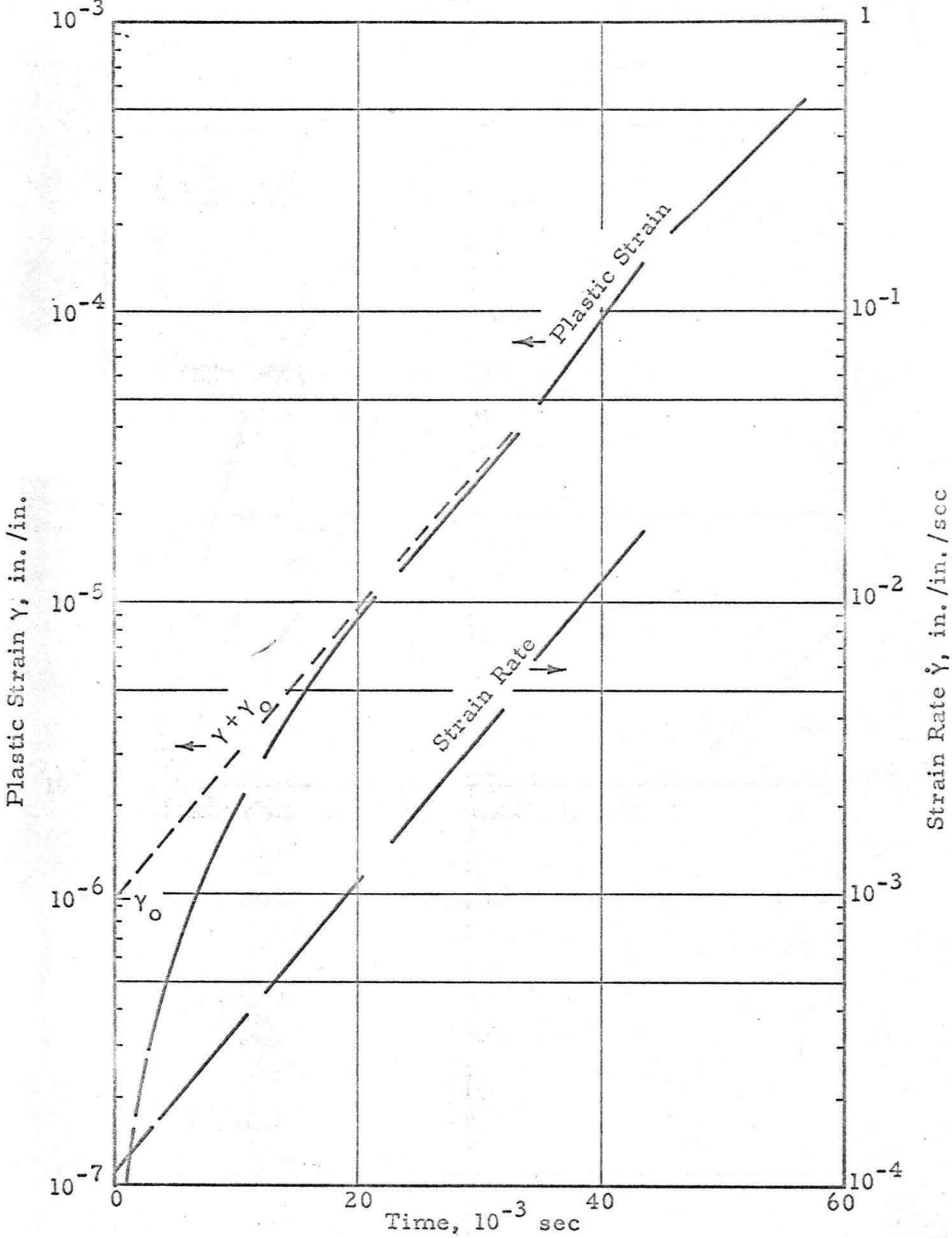

Fig. 12 Plastic Strain vs. Time and Strain Rate vs. Time. Specimen of 99.99 Per Cent Purity, 75°F. Applied Resolved Shear Stress 26.3 lb/in.^{2}, Interrupted.

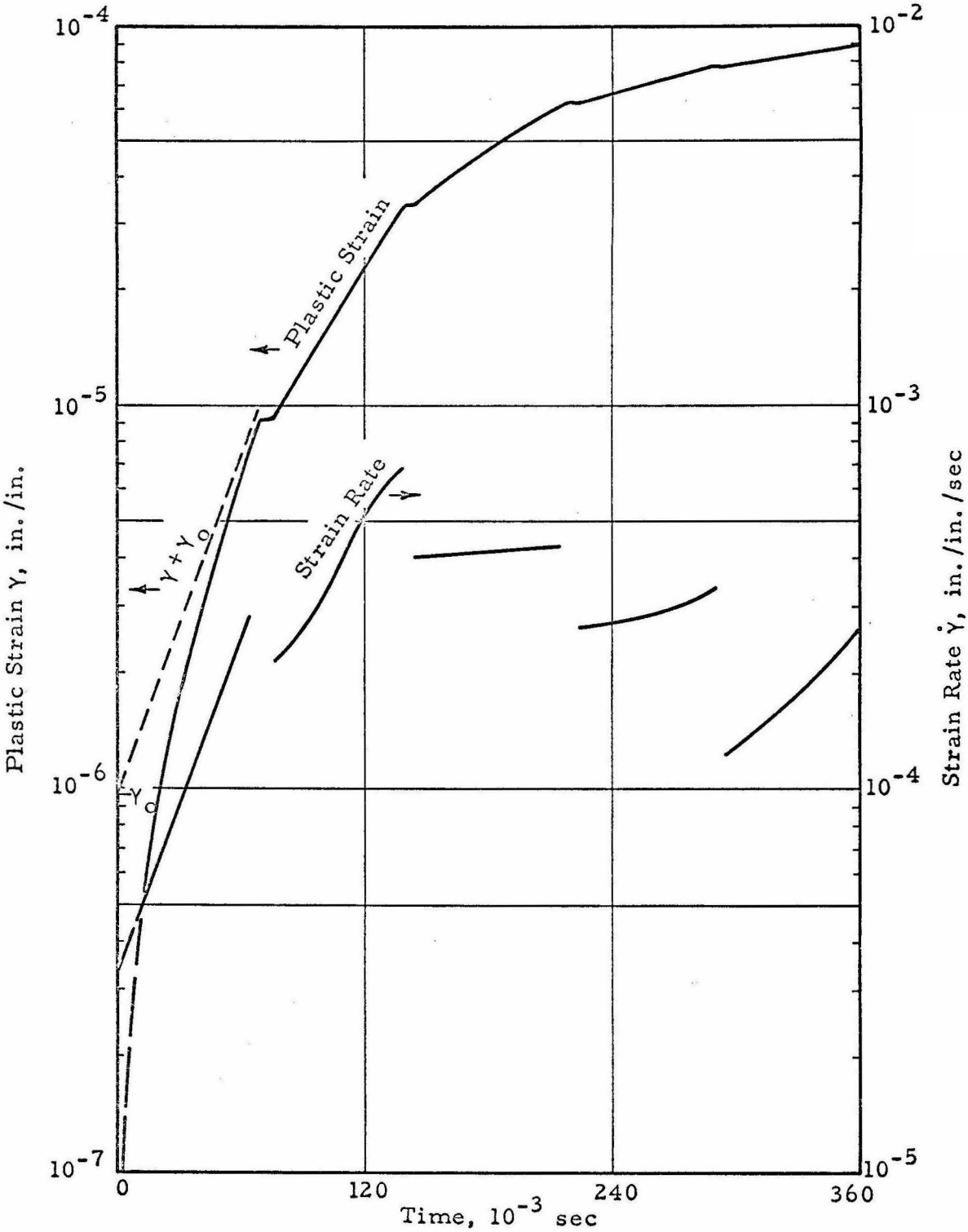

Fig. 13 Plastic Strain vs. Time and Strain Rate vs. Time. Specimen of 99.99 Per Cent Purity, -292°F. Applied Resolved Shear Stress 34.0 lb/in.^{2}.

TABLE II

Results of Rapid Loading Tests

Specimen No.	Specimen Purity (per cent)	Test Temperature (°F)	Static Yield Stress τ_y (lb/in.^{2})	Applied Shear Stress τ (lb/in.^{2})	Stress Increment $\tau-\tau_y$ (lb/in.^{2})	Log Strain Rate vs. Time: Slope $k\bar{v}$ (sec^{-1})	Log Strain Rate vs. Time: Intercept $\rho_o b\bar{v}$ (10^{-6} in./in. sec)	$\gamma_o \left(\frac{\rho_o b\bar{v}}{k\bar{v}}\right)$ (10^{-6} in./in.)
28	99.99 + nitrogen	75	31.5	46.7	15.2	490	123	0.25
				37.4	5.9	51.7	92	1.78
				36.7	5.2	21.7	7.5	0.35
		-93	40.0	51.7	11.7	421	93	0.22
				43.9	3.9	39.3	110	2.80
		-292	47.3	63.3	16.0	284	4,100	14.5
				54.6	7.3	99	350	3.54
30	99.99	75	17.4	35.0	17.6	460	1,130	2.46
				31.2	13.7	320	90	0.28
				29.8	12.4	271	69	0.25
				26.3	8.9	116	110	0.96
				25.8	8.4	98	190	1.92
				22.8	5.4	22.5	11.2	0.50
				22.5	5.1	23.0	18.2	0.79
		-93	20.1	34.7	14.6	245	560	2.3
				27.4	7.3	47	640	13.6
				25.7	5.8	24.2	510	21
		-292	27.1	39.1	12.0	395	2,600	6.6
				34.0	6.9	34.4	33	0.96

TABLE II (CONT.)

Results of Rapid Loading Tests

Specimen No.	Specimen Purity (per cent)	Test Temperature (°F)	Static Yield Stress τ_y (lb/in.^{2})	Applied Shear Stress τ (lb/in.^{2})	Stress Increment $\tau-\tau_y$ (lb/in.^{2})	Log Strain Rate vs. Time: Slope $\frac{\bar{kv}}{}$ (sec^{-1})	Log Strain Rate vs. Time: Intercept $\rho_o \bar{bv}$ (10^{-6} in./in. sec)	$\frac{Y_o}{\left(\frac{\rho_o \bar{bv}}{\bar{kv}}\right)}$ (10^{-6} in./in.)
36	99.999	75	16.2	29.4	13.2	299	13,000	43.5
37	99.999	75	15.1	30.0	14.9	509	9,000	17.8
38	99.999	75	15.2	29.2	14.0	393	3,200	8.15
				20.2	5.0	50	440	8.8
		-93	16.5	29.6	13.1	404	6,500	16.1
				19.2	2.7	15.6	119	7.6
39	99.999	75	15.2	29.7	14.5	500	3,500	7.0
				26.0	10.8	215	5,400	25.1
		-93	16.5	20.9	4.4	27.1	390	14.4

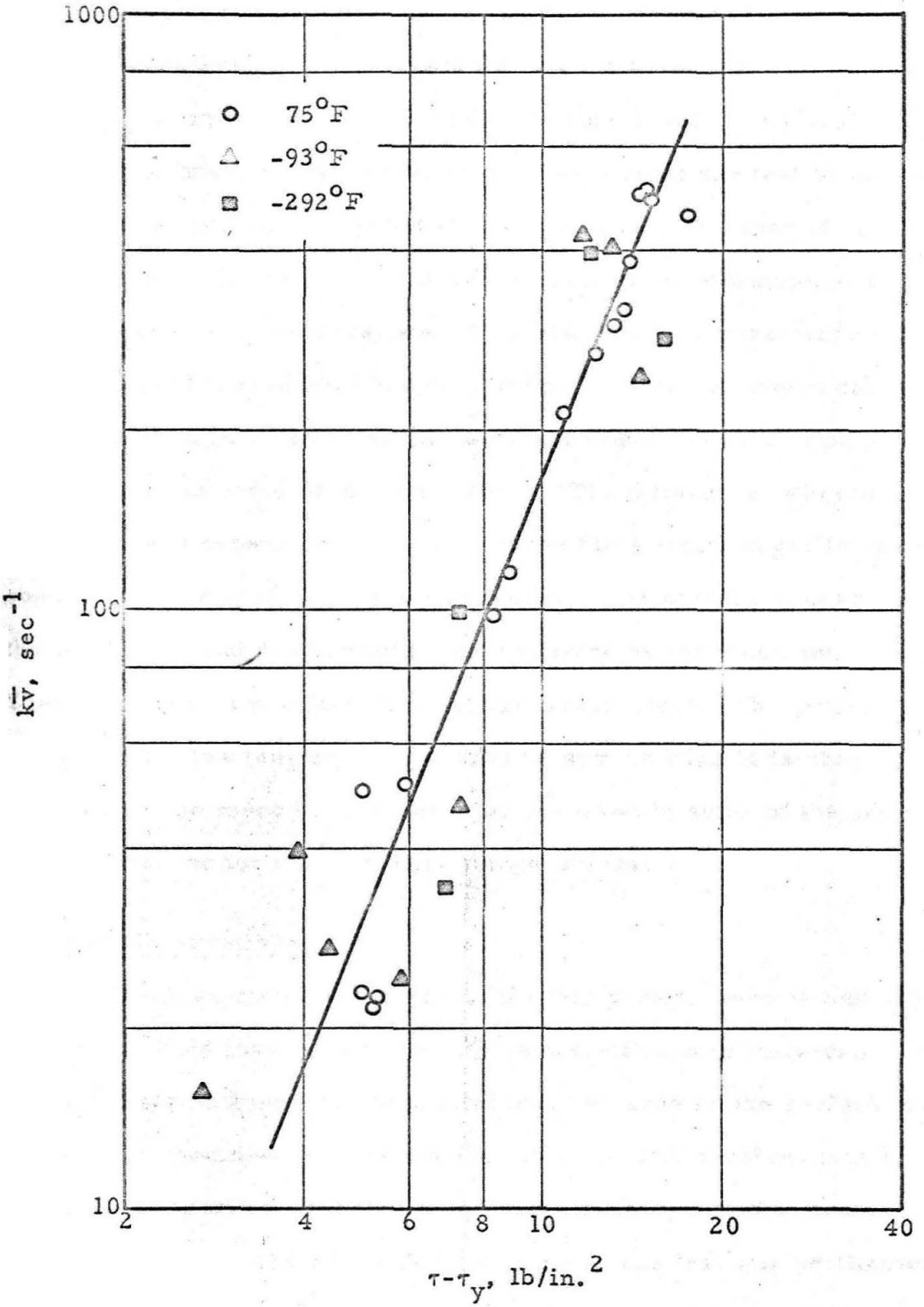

Fig. 14 Plot of $\bar{kv}$ vs. $(\tau-\tau_y)$.

the room temperature (75°F) tests and for the tests at higher values of $(\tau-\tau_y)$. Errors in the measurement of both τ and τ_y, as well as small variations in the specimens themselves from one test to the next, have a much larger effect at low values of $(\tau-\tau_y)$ than at the higher values. In the nitrogen doped specimen, for example, the yield stress in four successive static tests at room temperature was found to vary between 30.2 and 32.7 lb/in.^{2}. Such variations can have a relatively large effect in rapid load tests where the total applied stress is of the order of only 37 lb/in.^{2}. The difference between the coefficients of expansion of zinc and of the SR-4 strain gages is another source of error at the lower temperatures. The strain gages are of the paper type and are bonded to the specimen by Duco cement. Thermal stresses may also have a significant effect. The larger scatter of the low temperature results as seen in Fig. 14 is also reflected in the more erratic behavior observed in some of the strain vs. time curves for tests at these temperatures.

Etch-pip Observations

Three specimens, each of a different purity, were etched after their final rapid load tests to reveal the dislocations in the areas where the strain gages had been attached. An area on the surface of a deformed specimen is shown in Fig. 15a. A total resolved plastic shear strain of 375×10^{-6} in./in. had been recorded by the strain gages during the last test of this specimen. The test was performed at -93°F. Figure 15b is a photograph of the same area after the specimen had been annealed and re-etched. Approximately 0.010 to 0.020 in. was removed from the surface during the re-etching process.

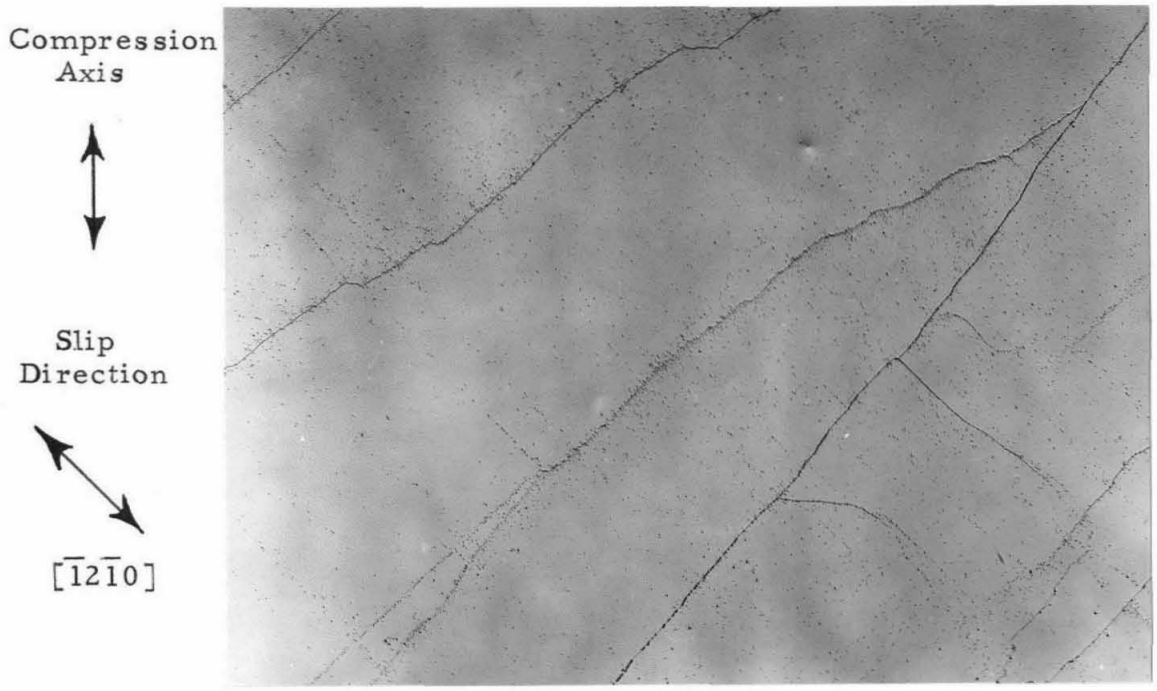

(a) After Rapid Loading Test at -93°F in which a Total Plastic Shear Strain of 375 x 10^{-6} in./in. was Measured.

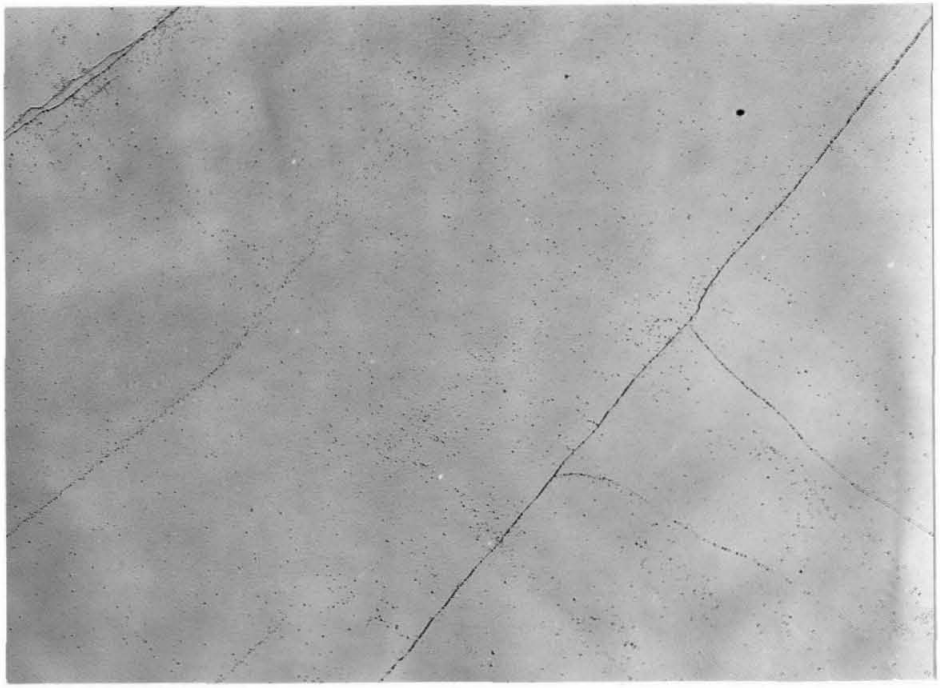

(b) Annealed in Vacuo at 700°F for 1 hr. and Re-etched.

Fig. 15 Etch-Pips on ($10\bar{1}0$) Plane in Nitrogen Doped Specimen, 100X.

The appearance of these areas is typical of many areas in all three specimens. Although considerable variation was observed in dislocation density and in the distribution and configuration of the small-angle boundaries, no major differences were observed between different specimens. Those small-angle boundaries which appear broader and more diffuse in the deformed specimens are seen to disappear upon annealing. The boundary in the center of Fig. 15a is an example of this type. The sharply defined boundaries are relatively unaffected by the annealing process. The boundary just to the right of center and both of the boundaries in the upper left corner in Fig. 15 are of this second type. (The one which appears to have disappeared was probably inclined at an angle to the surface so that the removal of a layer of zinc during the re-etching process caused the intersection between boundary and surface to shift toward the upper left corner.)

Several "representative" areas in the photographs of the nitrogen doped specimen were selected and etch-pip counts were made to determine the dislocation densities. These areas were chosen so as to exclude the sharply defined small angle boundaries. The counts for seven different areas in the deformed specimen gave values ranging from 5.0 to 26.4 x 10^5 cm^{-2}, with the average being 12.2 x 10^5 cm^{-2}. In the annealed specimen, counts made in approximately the same areas gave values ranging from 3.1 to 4.9 x 10^5 cm^{-2}, with an average of 4.2 x 10^5 cm^{-2}.

V. DISCUSSION OF RESULTS

A comparison of the static tests shown in Figs. 5, 6 and 7 shows the effect of purity and the addition of nitrogen on the yield stress and sharpness of the yield point in zinc. At 75°F (24°C) the yield stress of the nitrogen doped specimen is almost twice that of the other specimens, while the specimen of 99.99 per cent purity does not appear to be very much stronger than the specimen of 99.999 per cent purity. The yield point is the sharpest and most well defined in the nitrogen doped specimen. This specimen exhibits a plastic strain in excess of 2000 microin./in. at 75°F with no indication of the onset of work hardening. In the specimen of 99.99 per cent purity at this temperature, a plastic strain greater than 1000 microin./in. occurs with no increase of applied stress. In specimens of 99.999 per cent purity, little or no drop in applied stress is observed at yielding, and the strain proceeds slowly enough that it can be followed continuously on the strain indicator. Work hardening in these specimens can be detected after a strain of only a few hundred microin./in. Only one specimen of 99.99 per cent purity and one nitrogen doped specimen were studied; therefore the numerical results obtained for these specimens are not necessarily typical of the purities which they represent. The amount of impurity introduced into the nitrogen doped specimen could not be measured. There is a definite trend in the direction of increased strength and sharpness of yield with an increase in impurity content, however.

The effect of temperature on the three specimens is generally

the same. Both the yield stress and the work hardening rate increase with decreasing temperature. The increase in yield stress is greatest in the nitrogen doped specimen and least in the specimen of 99.999 per cent purity. The nitrogen doped specimen, which had the sharpest yield point at 75°F, has the smallest work hardening rate at the lower temperatures.

The strain vs. time curves obtained in the rapid load tests show a smooth and continuous increase of both strain and strain rate for all of the specimens studied and for all temperatures, from -292°F (-180°C) to +75°F (24°C). Thus, it is impossible to define a "delay time for the initiation of slip" without resorting to an arbitrary choice of an amount of plastic strain corresponding to the beginning of macroscopic yielding. No such choice is required in the case of polycrystalline steel and molybdenum because the strain vs. time curves exhibit two distinct regions and the delay time is defined by the transition from one region to the other. This difference in the general form of the two curves, together with the fact that grain boundaries are present in one case and not in the other, indicates that basically different mechamisms are operating in the two cases. Thus the concept of a delay time may have no real significance for zinc single crystals. Therefore, this interpretation will not be considered further, and the results of these experiments will be interpreted on the basis of an alternative mechanism.

Proposed Dislocation Mechanism

The dislocation mechanism chosen for this purpose is based upon the following assumptions:

1. There is an initial density, ρ_o, of weakly pinned dislocations in the annealed crystal which are free to move under the action of a shear stress $\tau > \tau_y$.
2. The average velocity, $\bar{v}$, of all dislocations taking part in the slip process at a given temperature is a function only of τ.
3. The total length of active dislocations per unit volume taking part in the slip process, ρ, increases in proportion to the total area of slip plane per unit volume that is swept out by the moving dislocations. (This is equivalent to the assumption that ρ increases linearly with increasing plastic strain.)

Assumption 2 is consistent with the experimental observation (1, 4) that individual dislocations in both lithium fluoride crystals and silicon-iron crystals accelerate very quickly and then move with constant velocity when a constant stress is applied to them. Assumption 3 is consistent with the observation (1, 18) that new dislocation loops form in lithium fluoride at many different sites in the wake of a moving dislocation and that the number of these new loops is proportional to the distance traveled by the original dislocation loop.

The third assumption gives the relation

$$\rho = \rho_o + kA, \tag{1}$$

where ρ_o is the total length of dislocation line per unit volume that

begins to move immediately when stress is applied, A is the total area of slip plane per unit volume swept by dislocations, and k is a constant. The resolved plastic shear strain, γ, in the crystal and the strain rate, $\dot{\gamma}$, expressed in terms of the motion of these dislocations, are

$$\gamma = Ab \tag{2}$$

and

$$\dot{\gamma} = \rho \bar{v} b, \tag{3}$$

where b is the Burgers vector and $\bar{v} = \bar{v}(\gamma)$ is the average dislocation velocity. Combining these equations,

$$\dot{\gamma} = \bar{v} b \left(\rho_o + \frac{k}{b} \gamma \right).$$

Integrating this equation gives

$$\log \left(\rho_o + \frac{k}{b} \gamma \right) = k \bar{v} t + c.$$

Then, since $\gamma = 0$ at $t = 0$, $C = \log \rho_o$, and hence

$$\gamma = \gamma_o \left(e^{k \bar{v} t} - 1 \right), \tag{4}$$

where

$$\gamma_o = \frac{\rho_o b}{k}.$$

The plastic strain rate is then given by

$$\dot{\gamma} = \rho_o b \bar{v} \, e^{k \bar{v} t}. \tag{5}$$

Equation 5 predicts that a plot of $\log \dot{\gamma}$ vs. t should be a straight line with slope $k\bar{v}$ and an intercept on the $t = 0$ axis of $\log(\rho_o b \bar{v})$. The

experimental results, as illustrated in Figs. 9-13, show that log $\dot{\gamma}$ vs. t is in fact quite linear up to strains of the order of 100 to 200 microin./in. Equation 4 predicts that a plot of log $(\gamma + \gamma_o)$ vs. t should also be a straight line. These plots are shown as dashed lines in Figs. 8-12, with the value for γ_o obtained by combining the values for $\rho_o b\bar{v}$ and $k\bar{v}$ from the respective plots of log $\dot{\gamma}$ vs. t .

Figure 10 shows that the behavior of the specimens of 99.999 per cent purity at 75°F (24°C) departs somewhat from Eq. 5 at the higher strain values. A similar difference between theory and experiment is observed in all specimens at the lower temperatures. This is probably due to a work hardening effect since the observed strain rates are less than the theoretical values after a certain amount of strain has taken place. There appears to be a definite correlation between this effect in the rapid load tests and the relative degrees of work hardening observed in the various static tests. Thus the theory applies only to the very early stages of plastic deformation before work hardening becomes significant.

The behavior predicted by the proposed mechanism agrees with the experimental results for all of the specimens and at all temperatures. This is an important result, and is of course a necessary prerequisite for the further consideration of the mechanism.

The linear relationship between the logarithm of the plastic strain rate and time simplifies the task of classifying and tabulating the experimental results. Each rapid load test can be described by

the two parameters, $k\bar{v}$ and $\rho_o b\bar{v}$, plus the specification of temperature, applied stress, and specimen tested. These values, for all the tests made in this investigation, are given in Table I. Figure 14 is a plot of log $k\bar{v}$ vs. log $(\tau-\tau_y)$. The figure shows that the experimental results for test specimens of all the degrees of purity investigated and for all test temperatures fall upon the same straight line, within experimental accuracy. This result, together with the results of the static tests, leads to the following conclusions:

1. The constant k must have the same value for all of the tests. If this were not so, k would have to vary linearly with $\bar{v}$ or it would have to depend upon $\tau-\tau_y$ in exactly the same way that $\bar{v}$ depends upon $\tau-\tau_y$, and in either case k would have to be otherwise unaffected by variations in temperature, purity and the absolute value of the applied stress. There is no reason to expect k and $\bar{v}$ to have a close interdependence.

2. The mean dislocation velocity, $\bar{v}$, depends only upon the excess of the applied stress, τ, over the static yield stress, τ_y.

3. The dependence of mean dislocation velocity upon crystal purity and temperature arises solely from the dependence of the static yield stress upon these variables.

4. The slope of the line in Fig. 14 gives the result that the average dislocation velocity increases with the 2.5 power of $\tau-\tau_y$.

Qualitatively, these conclusions agree in almost every respect with the findings of Gilman and Johnston (1, 2, 3, 19) regarding the behavior of individual dislocations in lithium fluoride and of Stein and Low (4) for silicon-iron. The effects of impurities and of changes in temperature have been studied in lithium fluoride, as well as the effects of radiation damage, strain hardening, and differing heat treatments. These various treatments all have an effect on the yield stresses of the crystals, often a very strong effect. Nevertheless in all cases the main effect of such changes is simply to shift the position of the curve of dislocation velocity vs. stress along the stress coordinate (when the dislocation velocity is plotted against the total applied stress rather than against the stress increment as in Fig. 14). The curves for crystals having different yield stresses are parallel to one another and the amounts of shift are found to be equal to the corresponding changes in the yield stress. Silicon-iron crystals behave in the same manner with respect to changes in temperature (4); namely, the yield stress increases at lower temperatures and this increase is accompanied by a corresponding increase in the stress required to produce a constant velocity of dislocation motion. The results of the present investigation show that the effects of temperature and purity upon the velocity of dislocation motion are qualitatively the same in zinc as in lithium fluoride and silicon-iron.

One qualitative difference between the results reported for lithium fluoride and the results of the present investigation concerns the observed rates of dislocation multiplication. The dislocation multiplication factor, k, in lithium fluoride was found to depend upon the

magnitude of the applied stress and upon the dislocation velocity. This investigation indicates that k for basal slip in zinc is independent of stress, dislocation velocity, purity, and temperature. In view of the many differences between these materials, and in view of the relatively small range of stresses and velocities covered in the present investigation, it is difficult to attach much significance to such a difference in behavior.

Additional evidence tending to confirm the proposed dislocation mechanism is provided by the results of the interrupted loading tests at 75°F, as illustrated in Fig. 12. This figure shows that after interruptions in loading the plastic strain begins again as if it had never been interrupted. This behavior is exactly what would be expected for dislocations that move with a constant velocity when subjected to a constant applied stress (assuming that none of the dislocations became pinned in some manner during the intervals between stress pulses). These results also imply that, at least for times of the order of 15 minutes, Cottrell (or impurity) pinning is not an important factor at 75°F.

At -93°F and at -292°F, interruptions in loading have a somewhat different effect. As was mentioned previously, however, the effect of the longer interruptions at these temperatures is not clear. Therefore only the short duration unloading pulses, as illustrated in Figs. 8b and 13, will be discussed. These unloading pulses appear to produce some pinning or entanglement of some of the dislocations in such a way that they are unable to move with the same freedom when the stress

returns to its original value. These dislocations then cease to participate in the slip process, thus reducing the overall rate of strain in the specimen. They also interfere with the motion of other dislocations, thus reducing the rate of increase of the strain rate. Since this effect is not observed at 75°F, the additional thermal energy at this temperature must be sufficient to dislodge the momentarily pinned dislocations. These low temperature pinning effects are observed to occur only when the unloading pressure pulses arrive at the specimen. Thus it appears that while a dislocation is in motion, unobstructed portions assist the applied stress in pulling other portions through the various local obstacles and retarding forces in the path of the dislocation. When the applied stress is temporarily reduced, however, many of these "unobstructed" portions are apparently allowed to fall back into lower energy positions which they had already passed and from which they must then be dislodged if the dislocation is to resume its motion. These same mechanisms may also be the cause of the higher work hardening rates observed in the static tests at -93°F and -292°F.

Determination of Density and Average Velocity of Moving Dislocations

An experimental determination of the dislocation multiplication factor k can be obtained by measuring the increase in the density of dislocations in a specimen subjected to a known amount of plastic strain. Thus, combining Eqs. 1 and 2:

$$k = \frac{b}{\gamma}(\rho - \rho_o) = \frac{b[\Delta\rho]}{[\gamma]} \qquad (6)$$

where $[\Delta\rho]$ and $[\gamma]$ are the measured values for the total net increase in dislocation density and the total plastic strain, respectively, in a given test. The value of ρ_o, the density of dislocations that move when stress is first applied, need not be known in order to determine k. This is a fortunate result, for it is almost certain that a large fraction of the dislocations in an annealed specimen will not take any part in the flow process. These include dislocations lying in other than the active slip planes, dislocations which lie in the active slip planes but whose Burgers vectors are not in the active slip direction, and dislocations which, although lying in the active slip planes and possessing the proper Burgers vector, are somehow pinned and held immobile. Because of the uncertainties in these quantities, particularly in the number of pinned dislocations, it would be extremely difficult to obtain a direct measurement of ρ_o based on etch-pip observations. An effective value for ρ_o may be obtained, however, from the measured values for $k\bar{v}$, $\rho_o b\bar{v}$ and k, as will be shown below.

The value of the dislocation multiplication constant, k, may be calculated from etch-pip observations by means of Eq. 6 provided that the annealing treatment is assumed to always return the specimen to the same state. The validity and necessity for this assumption has already been discussed. The average dislocation density in the nitrogen doped specimen after its final rapid load test was 12.2×10^5 cm^{-2}. After a standard annealing treatment, the average dislocation density was found to be 4.2×10^5 cm^{-2}. Taking the initial density in the undeformed specimen to be equal to the latter value, $[\Delta\rho]$ is

found to be 8.0×10^5 cm^{-2}. The total resolved plastic shear strain, $[\gamma]$, for this test was 375×10^{-6} in./in. Substituting these values into Eq. 6 gives

$$k = \frac{2.665 \times 10^{-8} \times 8.0 \times 10^5}{375 \times 10^{-6}} = 57 \text{ cm}^{-1}.$$

This is of the same order of magnitude as the values found by Johnston and Gilman (1) for the length of new dislocation line appearing in the wake of a moving dislocation in lithium fluoride.

The value of $k = 57$ cm^{-1} can now be employed, together with the experimentally determined quantities $[k\bar{v}]$ and $[\rho_o b\bar{v}]$, to obtain values for $\bar{v}$ and ρ_o for each test. Thus,

$$\bar{v} = \frac{[k\bar{v}]}{k} = \frac{[\gamma][k\bar{v}]}{b[\Delta\rho]} \tag{7}$$

and

$$\rho_o = \frac{k[\rho_o b\bar{v}]}{b[k\bar{v}]} = \frac{[\Delta\rho][\rho_o b\bar{v}]}{[\gamma][k\bar{v}]}. \tag{8}$$

The resulting values of $\bar{v}$ and ρ_o are presented in Table III.

The dislocation velocity $\bar{v}$ discussed above is the average velocity for all of the dislocations taking part in the plastic flow of the crystal. There are three factors which might cause the average velocity to differ from the velocities of the individual dislocations: 1) some of the moving dislocations might encounter obstacles, such as small angle boundaries, which they could not overcome and would thus be removed from participation in the plastic flow process; 2) the individual dislocations might move in a series of jumps rather than in

TABLE III

Experimental Values of $\bar{v}$ and ρ_o for k = 57 cm^{-1}

Specimen No.	Specimen Purity (per cent)	Test Temperature (°F)	Stress Increment $\tau - \tau_y$ ($lb/in.^2$)	$\bar{v}$ (cm/sec)	ρ_o (cm^{-2})
28	99.99	75	15.2	8.60	0.53×10^3
	+ nitrogen	75	5.9	0.91	3.80×10^3
		75	5.2	0.38	0.75×10^3
		-93	11.7	7.40	0.47×10^3
		-93	3.9	0.69	6.0×10^3
		-292	16.0	4.98	31.0×10^3
		-292	7.3	1.74	7.6×10^3
30	99.99	75	17.6	8.07	5.26×10^3
		75	13.7	5.71	0.60×10^3
		75	12.4	4.75	0.53×10^3
		75	8.9	2.04	2.06×10^3
		75	8.4	1.72	4.10×10^3
		75	5.4	0.39	1.07×10^3
		75	5.1	0.40	1.69×10^3
		-93	14.6	4.30	4.9×10^3
		-93	7.3	0.82	29.1×10^3
		-93	5.8	0.42	4.5×10^3
		-292	12.0	6.94	14.1×10^3
		-292	6.9	0.60	2.1×10^3
36	99.999	75	13.2	5.25	9.3×10^4
37	99.999	75	14.9	8.93	3.8×10^4

TABLE III (CONT.)

Specimen No.	Specimen Purity (per cent)	Test Temperature (^{o}F)	Stress Increment $\tau-\tau_y$ (lb/in.^{2})	$\bar{v}$ (cm/sec)	ρ_o (cm^{-2})
38	99.999	75	14.0	6.90	1.74×10^4
		75	5.0	0.88	1.88×10^4
		-93	13.1	7.09	3.44×10^4
		-93	2.7	0.27	1.63×10^4
39	99.999	75	14.5	8.77	1.50×10^4
		75	10.8	3.78	5.4×10^4
		-93	4.4	0.48	3.08×10^4

a uniform manner; and 3) edge dislocations and screw dislocations might move with different velocities when subjected to the same applied stress. Each of these possibilities will be considered.

The observed good agreement between the form of the experimental strain vs. time curve and the behavior predicted by the assumed dislocation mechanism suggests that the first possibility is not a significant factor during the early stages of plastic strain. If there were major obstructions to dislocation motion, such agreement would not be expected. (The obstructions may well be the cause of the deviations from the predicted behavior that occur later in the deformation process, however.) Any obstacles which have the effect of halting lengths of moving dislocations that are proportional to the total area of slip plane swept out would cause a reduction in the observed value of k but would not affect the value of $\bar{v}$.

The possibility that the dislocations may move in jerks rather than uniformly cannot be eliminated. The method by which $\bar{v}$ is deduced will not distinguish between these two possibilities. The methods used by Johnston and Gilman (1) to measure the velocities of individual dislocations in lithium fluoride are also unable to make this distinction. Thus, insofar as uniformity of dislocation motion is concerned, the values obtained for $\bar{v}$ in this investigation are comparable to the values obtained for the velocities of individual dislocations by means of the methods of Johnston and Gilman (1). Each of the individual dislocation velocity values reported by Johnston and Gilman is the average of 40 to 100 measurements, and there is often

considerable scatter of these measurements.

There is good reason to suspect that edge dislocations and screw dislocations in zinc do not move with the same velocity. Edge dislocations in lithium fluoride move about 50 times faster than screw dislocations for the same applied stress (1). Similarly, it has been inferred from the shapes of dislocation loops in silicon-iron that the edge components move much faster than the screw components (20). This possibility may be taken into account in the present investigation in the following manner. Consider an idealized dislocation loop in the slip plane which expands a small amount in time dt, as shown:

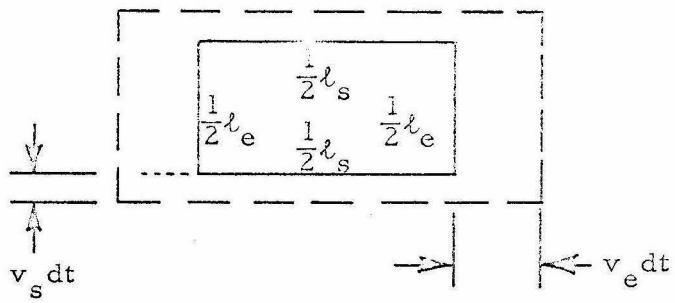

where

ℓ_s = length of screw dislocation

ℓ_e = length of edge dislocation

v_s = velocity of screw dislocation

v_e = velocity of edge dislocation.

The increase in length of the screw dislocations is

$$d\ell_s = 4v_e dt$$

and of the edge dislocations,

$$d\ell_e = 4v_s dt \ .$$

Thus

$$\frac{d\ell_s}{d\ell_e} = \frac{v_e}{v_s} \ .$$

Now, after any given loop has expanded to a size much larger than its size at birth, the ratio of total length of screw component to total length of edge component must be the same as the above ratio of increments of length. Therefore,

$$\frac{\rho_s}{\rho_e} = \frac{v_e}{v_s} = f, \tag{9}$$

where ρ_s is the density of moving screw dislocations and ρ_e is the density of moving edge dislocations.

The average dislocation velocity is then

$$\bar{v}^* = \frac{\rho_e v_e + \rho_s v_s}{\rho_e + \rho_s} = \left[\frac{1 + \left(\frac{\rho_s}{\rho_e}\right)\left(\frac{v_s}{v_e}\right)}{1 + \frac{\rho_s}{\rho_e}} \right] v_e = \left(\frac{2}{f+1} \right) v_e \ , \tag{10}$$

and the total density of moving dislocations is

$$\rho^* = \rho_e + \rho_s = (f+1)\rho_e \ . \tag{11}$$

The symbols with the asterisk signify that account has been taken of the fact that v_e and v_s may be different, and distinguish the values thus corrected from the corresponding uncorrected values.

Since a distinction is now being made between edge dislocations and screw dislocations, the method employed to obtain the values of $\bar{v}$ and ρ_o in Table III must be re-examined. These values were obtained

from Eqs. 7 and 8, and the quantity $\Delta\rho$ in these equations was determined by means of etch-pip counts. The observed increase in density of etch-pips actually corresponds to the increase in density of the edge components of the active dislocations, $\Delta\rho_e$. This follows from the relation which exists between the crystallographic plane on which the etch-pip observations were made and the Burgers vector of the active slip system. The relation between $\Delta\rho^*$ and $\Delta\rho_e$ can be obtained from Eq. 11. Thus,

$$\Delta\rho^* = (f+1)\Delta\rho_e \,. \tag{12}$$

Replacing $\Delta\rho$ in Eqs. 6, 7, and 8 by $\Delta\rho^*$ from Eq. 12,

$$k^* = (f+1)\frac{b[\Delta\rho_e]}{[\gamma]}, \tag{13}$$

$$\bar{v}^* = \left(\frac{1}{f+1}\right)\frac{[\gamma][k\bar{v}]}{b[\Delta\rho_e]}, \tag{14}$$

$$\rho_o^* = (f+1)\frac{[\Delta\rho_e][\rho_o b\bar{v}]}{[\gamma][k\bar{v}]}. \tag{15}$$

Therefore, in order to allow for the difference in velocities between edge dislocations and screw dislocations, the values of $\bar{v}$ and ρ_o in Table III must be multiplied by $\left(\frac{1}{f+1}\right)$ and $(f+1)$, respectively. Since the ratio of edge dislocation velocity to screw dislocation velocity in zinc is not known, this correction cannot be made at the present time. Substituting Eq. 10 into Eq. 14,

$$v_e = \frac{1}{2} \frac{[\gamma][k\bar{v}]}{b[\Delta\rho_e]} \quad . \tag{16}$$

Thus, under the assumptions employed in this analysis, the values of $\bar{v}$ in Table III are just twice the corresponding edge dislocation velocities, regardless of the velocities of the screw dislocations. The etch-pips observed on the crystal surface may represent mixed dislocations as well as pure edge dislocations, however. Therefore the observed value of $[\Delta\rho]$ probably includes dislocations with significant screw components. Thus $[\Delta\rho]$ is likely to be an overestimate of the increase in the density of edge dislocations. For this reason the values of $\bar{v}$ given in Table III are probably less than $2v_e$ and may be reasonably close to the true average dislocation velocity.

The above analysis represents a somewhat simplified picture of the situation. Nevertheless, it can be taken as a rough indication of the effect of differing edge and screw dislocation velocities on the values obtained for $\bar{v}$.

The numerical values obtained for $\bar{v}$ range from 0.4 cm/sec to about 9 cm/sec. The greatest distance traveled during a test by dislocations moving with these velocities would be of the order of 1 mm, which, on the scale of the photographs of Fig. 15, would be about 4 in. The average distance traveled would of course be much less than 1 mm because of the exponential nature of the increase in dislocation density. The general features of the etch-pip photomicrographs of the deformed specimens indicate that 1 mm is a reasonable order of magnitude for

the greatest distances traveled.

There is some variation in the values obtained for the initial density of moving dislocations, ρ_o, given in Table III. For the tests at 75°F ρ_o is of the order of 10^3 cm^{-2} in the nitrogen doped specimen and in the specimen of 99.99 per cent purity. The value of ρ_o is of the order of 10^4 cm^{-2} in the specimens of 99.999 per cent purity. These figures are consistent with the idea that many of the dislocations are pinned by impurities in the crystal and that in the specimens of 99.999 per cent purity there are fewer impurity atoms available and therefore more unpinned dislocations. The fact that ρ_o represents only about one per cent of the dislocations observed in an annealed crystal seems reasonable when compared with the results for lithium fluoride. Johnston and Gilman (1) reported that most of the dislocations present in an annealed lithium fluoride crystal did not move when a stress sufficient to move fresh dislocations was applied to the crystal. Various pinning effects involving fresh dislocations were also observed in lithium fluoride. The scatter of the ρ_o values in the low temperature tests is much greater than in the 75°F tests; ρ_o is often considerably larger at low temperatures than at 75°F. This fact is attributed largely to thermal stresses and the effects of the strain gages. Probably, in cases where ρ_o is unusually large, thermal stresses produced during cooling of the specimen have caused the unpinning of a significant number of dislocations or in the nucleation of a significant number of fresh dislocations.

Quantitative Comparisons Between Zinc, Lithium Fluoride, and Silicon-Iron

Data are not available for zinc with which the results of this investigation can be compared. The dislocation velocities obtained lie approximately in the center of the much wider range of velocities reported for lithium fluoride (10^{-7} cm/sec to 10^{5} cm/sec), and they are somewhat higher than the highest velocities obtained in silicon-iron (10^{-7} cm/sec to 10^{-2} cm/sec). The dislocation velocities reported in lithium fluoride (1) were plotted against the amount of the applied shear stress in excess of the yield stress of the crystal in order to compare the observed dependence of dislocation velocity upon stress in zinc with that in lithium fluoride. The velocity of edge dislocations in lithium fluoride, in the range from 10^{-1} cm/sec to 10 cm/sec, was found to increase approximately with the 4th power of $\tau-\tau_y$. The velocity of screw dislocations increases with the 5th power. The average dislocation velocity in zinc increases with the 2.5th power of $\tau-\tau_y$. Thus the stress dependence in zinc is somewhat weaker than in lithium fluoride. Since, at low velocities, the stress dependence in lithium fluoride is weaker than in silicon-iron, it is assumed that the stress dependence in zinc is weaker than that in silicon-iron as well.

Plastic Resistance

The results of this investigation indicate that dislocations in zinc move with a constant velocity when subjected to a constant applied stress. Further, the dislocation velocities are much less than the velocity of propagation of elastic shear waves. Therefore it must be assumed that the dislocations are subjected to a retarding force, or,

as Gilman terms it, a "plastic resistance", as they move through the crystal lattice. The origin of this retarding force and the means by which it produces the observed stress vs. velocity relation is not understood. However, given that such a force exists, certain properties can be ascribed to it on the basis of the observed experimental results, namely: (1) Below a certain level of applied stress, corresponding to the yield stress of the crystal, the plastic resistance is sufficient to prevent the dislocations from moving at all. (2) The plastic resistance is strongly affected by both the impurity content of the zinc and by temperature. (3) When the minimum stress required to cause yielding is exceeded, the plastic resistance acts as a constant drag force on the moving dislocations, causing them to move with an average velocity which depends only upon the magnitude of the applied stress in excess of the level needed to initiate yielding. These are the same properties which Gilman has attributed to the plastic resistance in lithium fluoride and silicon-iron.

The introduction of a new concept, such as "plastic resistance", always raises many new questions, and in the present case very few of these questions can as yet be answered. However, it appears that such a concept provides the only reasonable explanation for the observed results. The observed temperature dependence of the plastic strain rate would be difficult to explain on the basis of any dislocation pinning mechanism because all of the proposed mechanisms involve the assumption of a thermally activated release or generation of dislocations, so that the strain rate would be expected to vary with $\exp\left[-\frac{Q}{kT}\right]$.

Considered in terms of its dependence on $\tau-\tau_y$ (clearly an important factor no matter how the results are interpreted), the strain rate is not affected at all by temperature. The yield stress itself increases by only about 50 per cent while the temperature is reduced by a factor of 3.

VI. SUMMARY AND CONCLUSIONS

All of the specimens studied in this investigation were found to yield in a relatively smooth and continuous manner when subjected to a rapidly applied constant stress pulse. An abrupt change in strain rate that might be interpreted as a delay time for the initiation of macroscopic yielding was not found.

A dislocation mechanism has been proposed to relate the observed macroscopic plastic strain vs. time behavior of zinc to the motion of the individual dislocations in the crystal. This mechanism is based upon the assumptions that there is an initial density of weakly pinned dislocations in the annealed crystal which are free to move under the action of an applied stress greater than the yield stress of the crystal; that the average velocity of the moving dislocations depends only upon the magnitudes of the applied stress and the temperature; and that the dislocation density increases in proportion to the area swept out by the moving dislocations. The theory of the proposed dislocation mechanism contains three unknown quantities:

1. the density of weakly pinned dislocations that move immediately upon stress application,
2. the average dislocation velocity,
3. the proportionality constant between the increase in density of moving dislocations and the amount of plastic strain.

The experimental measurements of plastic strain vs. time provide the following results:

1. The exponential form of the experimental plastic strain vs. time curves agree with the form predicted from the proposed dislocation mechanism.
2. Each experimental plastic strain vs. time relation provides two quantitative relationships between the three unknown quantities that appear in the theory. A third quantitative relationship between the three theoretical quantities is obtained from measurements of dislocation densities by means of etch-pip techniques. Thus quantitative values for each of the three theoretical quantities may be obtained from the experimental measurements. The numerical values thus obtained are of reasonable orders of magnitude and, when taken as a whole, provide an internally consistent basis for the interpretation of all of the various phenomena observed. Values for the average dislocation velocity range from 0.4 to 9 cm/sec. These "average" values tend to approach a value that is twice the velocity of edge dislocations in zinc for the idealized case in which the dislocation loops are composed of pure edge and pure screw dislocations. The initial density of unpinned dislocations (those which move immediately upon the application of stress) was found to be of the order of 10^4 cm^{-2} in the specimens of highest purity. The dislocation density in specimens of lower purity was $\sim 10^3$ cm^{-2}.

3. When the average dislocation velocity for each test is plotted against the increment in the applied shear stress above the static yield stress, $\tau-\tau_y$, the points for all tests fall along a single line. This result implies that the average dislocation velocity depends only upon the quantity $\tau-\tau_y$, regardless of the impurity content of the zinc or the temperature at which the test is performed. Thus $\tau-\tau_y$ is a parameter of considerable importance in the determination of the yield behavior of zinc.
4. The yield stress of zinc, τ_y, is strongly dependent upon both purity and temperature.
5. In the stress range studied, the average dislocation velocity increases with the 2.5 power of the stress increment, $\tau-\tau_y$.

The above interpretation is in complete agreement with the original assumptions of the proposed mechanism and it yields reasonable and internally consistent numerical results. The stress dependence of the average dislocation velocity obtained under this interpretation agrees qualitatively in every respect with the observed behavior of individual dislocations in lithium fluoride and silicon-iron (the only materials in which such measurements have been made). On the basis of these observations, it is concluded that the concept of a lattice resistance to dislocation motion or a "plastic resistance", can be applied to the yield behavior of zinc as well as to lithium fluoride and silicon-iron, and that in fact this appears to be the only consistent interpretation of the observed results.

REFERENCES

1. W. G. Johnston and J. J. Gilman, "Dislocation Velocities, Dislocation Densities, and Plastic Flow in Lithium Fluoride Crystals", Journal of Applied Physics, Vol. 30 (1959), pp. 129-144.

2. J. J. Gilman, "The Plastic Resistance of Crystals", Australian Journal of Physics, Vol. 13 (1960), pp. 327-346.

3. J. J. Gilman and W. G. Johnston, "Behavior of Individual Dislocations in Strain-Hardened LiF Crystals", Journal of Applied Physics, Vol. 31 (1960), pp. 687-692.

4. D. F. Stein and J. R. Low, Jr., "Mobility of Edge Dislocations in Silicon-Iron Crystals", Journal of Applied Physics, Vol. 31 (1960), pp. 362-369.

5. D. S. Clark and D. S. Wood, "The Time Delay for the Initiation of Plastic Deformation at Rapidly Applied Constant Stress", Proceedings, American Society for Testing Materials, Vol. 49 (1949), pp. 717-735.

6. J. A. Hendrickson, D. S. Wood, and D. S. Clark, "The Initiation of Discontinuous Yielding in Ductile Molybdenum", Transactions of American Society for Metals, Vol. 48 (1956), pp. 540-558.

7. T. Vreeland, Jr., D. S. Wood, and D. S. Clark, "Preyield Plastic and Anelastic Microstrain in Low-Carbon Steel", Acta Metallurgica, Vol. 1 (1953), pp. 414-421.

8. T. L. Russell, D. S. Wood, and D. S. Clark, "The Influence of Grain Size on the Yield Phenomenon in Steel", Acta Metallurgica, Vol. 9 (1961), pp. 1054-1063.

9. I. R. Kramer and R. Maddin, "Delay Time for the Initiation of Slip in Metal Single Crystals", Transaction of American Institute of Mining, Metallurgical and Petroleum Engineers, Vol. 194 (1952), pp. 197-203.

10. T. S. Liu, I. R. Kramer and M. A. Steinberg, "The Delay-Time Phenomenon in Metal Single Crystals", Acta Metallurgica, Vol. 4 (1956), pp. 364-370.

11. I. R. Kramer, "Dislocation Blocking in Face-Centered-Cubic Metals", Transactions of American Institute of Mining, Metallurgical and Petroleum Engineers, Vol. 215 (1959), pp. 226-230.

12. I. R. Kramer, "Delay Time in Single Crystals of Aluminum, Zinc, and Iron", Transactions of American Institute of Mining, Metallurgical and Petroleum Engineers, Vol. 221 (1961), pp. 474-478.

13. K. R. King, "Study of the Yield Phenomenon in Zinc Single Crystals", Fourth Technical Note under Air Force Office of Scientific Research, Contract No. AF 18(600)-490, California Institute of Technology, 1958.

14. H. L. Wain and A. H. Cottrell, "Yield Points in Zinc Crystals", Proceedings, Physical Society, Vol. 633 (1950), pp. 339-345.

15. E. J. Stofel, "Plastic Flow and Fracture of Zinc Single Crystals", Ph.D. Thesis, California Institute of Technology, 1962.

16. C. H. Li, J. Washburn, and E. R. Parker, "Variation of Plastic Properties with Annealing Procedure in Zinc Single Crystals", Transactions of American Institute of Mining, Metallurgical and Petroleum Engineers, Vol. 197 (1953), pp. 1223-1225.

17. R. C. Brandt, K. H. Adams and T. Vreeland, Jr., "Etching of High Purity Zinc", First Technical Report under Office of Naval Research, Contract No. Nonr-220(37), California Institute of Technology, 1961.

18. W. G. Johnston and J. J. Gilman, "Dislocation Multiplication in Lithium Fluoride Crystals", Journal of Applied Physics, Vol. 31 (1960), pp. 632-643.

19. J. J. Gilman and W. G. Johnston, "Dislocations, Point-Defect Clusters, and Cavities in Neutron Irradiated LiF Crystals", Journal of Applied Physics, Vol. 29 (1958), pp. 877-888.

20. J. R. Low, Jr., and R. W. Guard, "The Dislocation Structure of Slip Bands in Iron", Acta Metallurgica, Vol. 7 (1959), pp. 171-179.